



Review

# Membrane Separation Technology in Direct Air Capture

Pavlo Ignatusha <sup>1,2</sup>, Haiqing Lin <sup>3,\*</sup> , Noe Kapuscinsky <sup>1,4</sup> , Ludmila Scoles <sup>1</sup>, Weiguo Ma <sup>1</sup>,  
Bussaraporn Patarachao <sup>1</sup> and Naiying Du <sup>1,\*</sup>

- <sup>1</sup> Energy, Mining and Environment Research Center, National Research Council of Canada, Ottawa, ON K1A 0R6, Canada; noe.kapuscinsky@nrc-cnrc.gc.ca (N.K.); ludmila.scoles@nrc-cnrc.gc.ca (L.S.)
- <sup>2</sup> Department of Biochemistry, Microbiology and Immunology, University of Ottawa, Ottawa, ON K1N 6N5, Canada
- <sup>3</sup> Department of Chemical and Biological Engineering, University at Buffalo, The State University of New York, Buffalo, NY 14260, USA
- <sup>4</sup> Department of Chemical and Biological Engineering, University of Ottawa, Ottawa, ON K1N 6N5, Canada
- \* Correspondence: haiqingl@buffalo.edu (H.L.); naiying.du@nrc-cnrc.gc.ca (N.D.)

**Abstract:** Direct air capture (DAC) is an emerging negative CO<sub>2</sub> emission technology that aims to introduce a feasible method for CO<sub>2</sub> capture from the atmosphere. Unlike carbon capture from point sources, which deals with flue gas at high CO<sub>2</sub> concentrations, carbon capture directly from the atmosphere has proved difficult due to the low CO<sub>2</sub> concentration in ambient air. Current DAC technologies mainly consider sorbent-based systems; however, membrane technology can be considered a promising DAC approach since it provides several advantages, e.g., lower energy and operational costs, less environmental footprint, and more potential for small-scale ubiquitous installations. Several recent advancements in validating the feasibility of highly permeable gas separation membrane fabrication and system design show that membrane-based direct air capture (m-DAC) could be a complementary approach to sorbent-based DAC, e.g., as part of a hybrid system design that incorporates other DAC technologies (e.g., solvent or sorbent-based DAC). In this article, the ongoing research and DAC application attempts via membrane separation have been reviewed. The reported membrane materials that could potentially be used for m-DAC are summarized. In addition, the future direction of m-DAC development is discussed, which could provide perspective and encourage new researchers' further work in the field of m-DAC.



**Citation:** Ignatusha, P.; Lin, H.; Kapuscinsky, N.; Scoles, L.; Ma, W.; Patarachao, B.; Du, N. Membrane Separation Technology in Direct Air Capture. *Membranes* **2024**, *14*, 30. <https://doi.org/10.3390/membranes14020030>

Academic Editor: Adolfo Iulianelli

Received: 12 December 2023

Revised: 16 January 2024

Accepted: 17 January 2024

Published: 24 January 2024



**Copyright:** © 2024 by the authors. Licensee MDPI, Basel, Switzerland. This article is an open access article distributed under the terms and conditions of the Creative Commons Attribution (CC BY) license (<https://creativecommons.org/licenses/by/4.0/>).

**Keywords:** direct air capture; membrane; carbon dioxide; high permeance

## 1. Introduction

The terms climate change and climate action have been on the tip of everyone's tongues for the last few years. Although carbon capture is a promising start, with the carbon budget clock ticking away, it is clear that simply lowering emissions, e.g., capturing CO<sub>2</sub> from point sources, will not make enough of an impact. It is not long until the carbon budget is depleted, and every additional ton of CO<sub>2</sub> will need to be managed by the use of negative emission technologies [1,2]. In fact, in order to meet the Paris Climate Agreement goals of preventing a 1.5–2 °C temperature increase over preindustrial levels, 10 GtCO<sub>2</sub>/yr will need to be removed from the atmosphere by the midcentury, increasing to 20 GtCO<sub>2</sub>/yr by the end of the century [3]. Failing to prevent the increase in temperature has a very real social cost. For example, wheat, rice, maize, and soybean represent over 67% of human caloric intake; only a 1 °C increase in temperature will reduce the global production of wheat by 6%, rice by 3%, maize by 7.4%, and soybean by 3.1% [4]. Additionally, changes in weather patterns, acidification of oceans, and melting of polar ice caps place much of the planet's biodiversity at risk. Therefore, the development of cost-effective negative emission technologies becomes essential to remediate climate change. As one of the negative emission technologies, direct air capture (DAC) describes a

process by which CO<sub>2</sub> is removed directly from the atmosphere rather than from higher concentration point sources. This proves to be quite challenging as the concentration of CO<sub>2</sub> in the atmosphere is only ~400 ppm [5]. Nonetheless, it is important to develop methods to capture low-concentration atmospheric CO<sub>2</sub> since capturing all emissions from point sources would fail to accomplish even an 80% emission reduction by 2050 [6], while direct air capture would be able to target the CO<sub>2</sub> from the billions of small point sources which account for 1/3 to 1/2 of society's CO<sub>2</sub> emissions [7].

Currently, sorbent-based DAC technologies are under development at a pilot scale, including solid sorbents and liquid solvents [8,9]. These two technologies rely on absorption/desorption technologies, which require high energy inputs and large location-dependent installations. In addition, these processes often involve the use of chemicals and, therefore, introduce added environmental and safety risks [5,9–12]. Liquid solvent DAC utilizes contactors where the gas encounters a basic solution. The resulting compounds need intense heating to release captured CO<sub>2</sub> [8,11,13]. Because of the use of strong bases, the sorbent liquids are usually no more than 30% concentrated, which greatly decreases their binding potential with CO<sub>2</sub> [14]. The use of strong chemicals, e.g., KOH, also risks a negative environmental impact in the form of spills. In addition, liquid solvents use 1–7 tons of water to capture 1 ton of CO<sub>2</sub> [9]. Recent research on liquid solvent-based DAC focuses on lowering the consumption of energy and water, e.g., IPDA (3-(aminomethyl)-3,5,5-trimethylcyclohexylamine) liquid to solid carbamic acid conversion for CO<sub>2</sub> which can capture low (400 ppm) CO<sub>2</sub> with >99% removal at a lower desorption temperature of 333 K [15]. Solid sorbent methods involve pushing air into a specially designed sorbent until it is saturated. The sorbent is then heated and/or vacuumed to desorb CO<sub>2</sub> [14]. Solid sorbents have been made of several different materials like metal-organic frameworks (MOFs), mixed metal oxides, poly(ethylenimine) etc. [16]. Metal-organic frameworks are formed through the linkage of organic and inorganic constituents, which form highly structured and microporous materials with high free volumes. The performance of solid sorbent DAC depends on the conditions of the air being processed, including temperature and humidity. High temperatures have been shown to increase energy requirements, leading to a loss of efficiency and an increase in cost [17]. These factors lead to location dependence for DAC installation for both technologies. The source of energy used to power these sorbent-based DAC plants must also be considered when evaluating their level of negative emissions and may limit the location even more [9]. The KOH liquid absorption method reportedly requires 8.81 GJ of natural gas or 5.25 GJ of gas and 366 kWh of electricity for every ton of CO<sub>2</sub> captured [11]. Solid sorbent energy requirements are around 6 GJ of thermal energy and 1.5 GJ of electricity per ton of CO<sub>2</sub> [14]. These energy demands arise primarily due to the desorption steps. Although sorbent-based DAC technologies being developed to a plant scale is a great start and is paving a path for DAC, the impact on the environment should not be underestimated, and other environmentally friendly approaches should be explored.

The idea of m-DAC was proposed twenty years ago [18]; however, only recently has a more detailed study been reported that proved that membrane processes could be considered as a new DAC approach [5]. It is a new and rather exciting area of research that shows promise for lower-cost direct air carbon capture and can lower the risk of environmental impact associated with sorption technologies [5]. Theoretically, considering the process only requires energy to blow air through the membranes, advances in membrane materials should drastically decrease the cost of operation, especially given that thermodynamic energy requirements are 20–30 times lower than that of the best DAC methods currently in use [19,20]. However, presently, m-DAC will not be a competitive option to sorbents-based DAC unless major breakthroughs are made in increasing membrane selectivity for the CO<sub>2</sub>:N<sub>2</sub> gas pair and CO<sub>2</sub> permeance. Currently, it is widely accepted that m-DAC could play an active role in hybrid system designs that incorporate other DAC technologies. In the past few decades, large amounts of funding have been allocated worldwide for the R&D of membrane-based CO<sub>2</sub> capture from point sources, and a vast number of published reports

related to high permeable polymeric materials for CO<sub>2</sub> capture membranes could shed light on the selection of DAC membrane materials. Rather than introducing the m-DAC hybrid system, this review gives a perspective of the most recent research on membrane-based direct air capture systems and potential polymeric membrane materials for DAC. Although there is currently very little literature on m-DAC, given its novelty, this review intends to illustrate the need for membrane DAC research and encourage researchers in the field to explore further.

## 2. Feasibility of m-DAC

Although membrane separation is a promising technology for capturing CO<sub>2</sub> and, to date, a few pilot plants for point source CO<sub>2</sub> capture have been operated; the pervasive belief is that m-DAC was implausible because the concentration of CO<sub>2</sub> in the air is only about 400 ppm which leads to an insufficient driving force for CO<sub>2</sub> permeation through the membranes [21].

Recent achievements in polymer membrane materials with ultrahigh gas permeance and selectivity have exposed the silver lining that membrane separation could potentially be applied in DAC processes. Fujikawa et al. explored the potential of m-DAC based on process simulation with consideration of the state-of-the-art CO<sub>2</sub> separation membrane performance. The results of the four-stage separation could encourage researchers to explore more realistic membrane performances and process conditions for m-DAC. In their incredibly comprehensive modeling study, they modeled a 4-stage separation process after highly permeable membranes (CO<sub>2</sub> Permeance of 40,000 GPU (Gas Permeation Unit (GPU) =  $3.35 \times 10^{-10} \frac{\text{mol}}{\text{m}^2 \cdot \text{s} \cdot \text{Pa}}$ ) and CO<sub>2</sub>/N<sub>2</sub> selectivity of 70) and showed that a CO<sub>2</sub> concentration of ~30% was achievable at the final stage of a four-stage system with only a membrane area of ~3.2 m<sup>2</sup>/kg CO<sub>2</sub>/day (as a flat sheet) and 16 kWh/kg-CO<sub>2</sub>/day. Their model system assumed a feed pressure of 101.3 kPa and a permeate pressure of 5 kPa and maintained a pre-industrial retentate CO<sub>2</sub> concentration of ~300 ppm [12].

## 3. Considerations for m-DAC

Direct air capture by membranes depends on several factors, which include membrane properties as well as process parameters.

### 3.1. Permeance

Gas permeance is a measure of the gas transport ability of a material at a given thickness; therefore, it depends on the permeability and thickness of the membrane. Separation by membranes typically follows the Solubility-Diffusion model, which is based on the solubility and diffusion rate of gases going through the membrane [22,23]. Some membranes are capable of facilitated transport mechanisms where carriers react reversibly with CO<sub>2</sub> selectively, while other gasses only cross by the Solubility-Diffusion mechanism at a lower rate. As a result, these membranes offer high selectivity and gas permeance [24].

$$P = \frac{K}{l} \quad (1)$$

$$K = S \times D \quad (2)$$

Membranes with a high Solubility-Diffusion relationship and low thickness are candidates for increased permeance based on Equations (1) and (2) where  $P$  is gas permeance,  $K$  is permeability (Barrer =  $3.35 \times 10^{-10} \frac{\text{mol} \cdot \text{m}}{\text{m}^2 \cdot \text{s} \cdot \text{Pa}}$ ),  $l$  is membrane thickness,  $S$  is solubility and  $D$  is diffusion rate. For power plant post-combustion CO<sub>2</sub> capture, Merkel et al. concluded that improved gas permeance in membranes is more critical for reducing capture cost than enhanced selectivity [20]. While selectivity is also extremely crucial for DAC, only membranes with high permeance can be considered as an attractive option for DAC. Thinning of membranes is a large area of research for increasing permeance. The thickness of DAC membranes should be reduced to the nanometer level in order to increase membrane permeance significantly because the required membrane area is inversely proportional

to permeance. However, it should be noted that studies have shown permeability has a tendency to decrease for many materials in the submicron range, which can lead to a decrease in permeance [25,26].

### 3.2. Selectivity

Membrane gas selectivity ( $\text{CO}_2/\text{N}_2$ ) is of great interest for m-DAC design, given that nitrogen is the largest component of the earth's atmosphere and the  $\text{CO}_2$  concentration is only about 400 ppm. Ideal gas selectivity is defined as the ratio of  $\text{CO}_2$  to  $\text{N}_2$  permeability, as shown below.

$$\alpha_{\text{CO}_2/\text{N}_2} = \frac{K_{\text{CO}_2}}{K_{\text{N}_2}} \quad (3)$$

where  $\alpha$  is the selectivity,  $K_{\text{CO}_2}$  is  $\text{CO}_2$  permeability and  $K_{\text{N}_2}$  is  $\text{N}_2$  permeability in single gas tests [27]. The determination of selectivity becomes more complicated when it comes to mixed gas testing. Low selectivity leads to a higher migration of unwanted gases and a lower concentration of  $\text{CO}_2$  in the permeate. As a rule of thumb, permeance should be maximized to decrease membrane area [12], but selectivity should be optimized as membranes with a selectivity that is too high require more membrane area and show little benefit in  $\text{CO}_2$  purity. Merkel et al. compared two membranes for point source  $\text{CO}_2$  capture, the "best case" membrane and membrane B. The "best case" membrane had a  $\text{CO}_2$  permeance of 1000 GPU and a  $\text{CO}_2/\text{N}_2$  selectivity of 50, while membrane B had a  $\text{CO}_2$  permeance of 1000 GPU and a  $\text{CO}_2/\text{N}_2$  selectivity of 200. They found that the best-case membrane produced a permeate with 46%  $\text{CO}_2$  at 2.1 MM m<sup>2</sup>, while membrane B yielded 55%  $\text{CO}_2$  with an area nearly three times larger at 5.7 MM m<sup>2</sup> [20]. The concentration of  $\text{CO}_2$  in the permeate increases greatly with selectivity until a selectivity of about 30 when it begins to plateau. The selectivity also decreases the energy required for vacuuming, which similarly plateaus. Fujikawa et al. showed that a membrane with a  $\text{CO}_2$  permeance of 10,000 GPU and a  $\text{CO}_2/\text{N}_2$  selectivity of 50 could reach 66.7%  $\text{CO}_2$  with only 4.63 m<sup>2</sup>/kg  $\text{CO}_2$ /day and ~12.3–16 kWh/kg- $\text{CO}_2$ /day at a pressure ratio of 50 using a feed pressure of 110 kPa and a permeate pressure of 2 kPa. The membrane area required increases with selectivity almost linearly while the benefits in  $\text{CO}_2$  concentration, energy requirement, and  $\text{CO}_2$  emission related to the energy production decrease with each 10-step selectivity increase [12].

Although less important than the previous two parameters,  $\text{CO}_2/\text{O}_2$  selectivity should also be considered depending on downstream applications of captured  $\text{CO}_2$  as processes like the reduction of  $\text{CO}_2$  to  $\text{CO}$  and  $\text{CH}_4$  are typically hindered due to the oxidative pressures of  $\text{O}_2$  [12].

### 3.3. Pressure Ratio

The pressure ratio is feed pressure divided by permeate pressure.

$$\varphi = \frac{p_f}{p_p} \quad (4)$$

$$X_p \leq X_f \times \varphi \quad (5)$$

where  $p_f$  and  $p_p$  are feed and permeate pressures respectively. Equation (5), where  $X_p$  is the mol fraction in the permeate and  $X_f$  is the mol fraction in the feed, shows that the mole fraction of  $\text{CO}_2$  on the permeate side is limited by the pressure ratio independently of other parameters, notably selectivity [12,23]. For flux across the membrane in the desired direction, the partial permeate  $\text{CO}_2$  pressure cannot exceed the partial feed  $\text{CO}_2$  pressure in order to maintain a favorable cross-membrane pressure gradient. Because the mole fraction in the permeate is limited proportionally by the pressure ratio, a higher pressure ratio leads to greater permeate  $\text{CO}_2$  concentrations. The largest effect of pressure ratio on  $\text{CO}_2$  permeate concentration is observed under  $\varphi = 30$ , after which the effect begins to plateau [12]. Vacuuming processes have been shown to be more energy efficient than feed compression systems for gas separation [23].

Fujikawa et al. studied the effect of pressure ratio on m-DAC via process simulation with the same CO<sub>2</sub> retentate concentration (~300 ppm) and the same membrane (permeance of 40,000 GPU and selectivity of 70) (Table 1); however, the pressure ratio is different. When the pressure at the permeate side is 4 kPa ( $\varphi = 25$ ), the final CO<sub>2</sub> concentration can exceed 40%. Membrane area and CO<sub>2</sub> emissions related to the energy production decrease from 3.19 to 2.6 m<sup>2</sup>/kg-CO<sub>2</sub>/day and 0.6 to 0.54 kgCO<sub>2</sub><sup>emitted</sup>/kgCO<sub>2</sub><sup>captured</sup>, respectively, when the pressure ratio is raised from 20 to 25. It is important to note that at each stage, the energy and membrane area required falls dramatically when compared to the first stage. This illustrates the importance of process parameters in addition to material properties like permeance and selectivity.

**Table 1.** The m-DAC separation outcomes with different pressure ratios [12]. Data for the Pressure ratio of 20 is summated while the pressure ratio of 25 is not (each stage).

Number of Separation Stages	Pressure Ratio = 20 Permeate Pressure = 5 kPa					Pressure Ratio = 25 Permeate Pressure = 4 kPa				
	1	2	3	4	Total	1	2	3	4	Total
CO <sub>2</sub> concentration in permeate (%)	0.6	2.9	10.8	29.8	-	0.7	3.9	15.5	42.4	-
Membrane area (m <sup>2</sup> /kg-CO <sub>2</sub> /day)	2.57	(0.47)	(0.12)	(0.03)	3.19	2.15	0.35	0.08	0.02	2.6
Energy required for vacuuming (kWh-CO <sub>2</sub> /day)	12.7	(2.4)	(0.7)	(0.2)	16.0	11.6	1.9	0.5	0.2	14.2
CO <sub>2</sub> emission related to the energy production (kgCO <sub>2</sub> <sup>emitted</sup> /kgCO <sub>2</sub> <sup>captured</sup> )	0.48	(0.09)	(0.02)	(0.01)	0.6	0.44	0.07	0.02	0.01	0.54

### 3.4. Stage Cut

Stage cut is defined as permeate flow divided by feed flow.

$$\varnothing = \frac{f_p}{f_f} \quad (6)$$

where  $\varnothing$  is Stage cut and  $f_p$  and  $f_f$  are permeate and feed flows, respectively [12,28]. A high feed flow leads to a lower change in feed gas concentrations, which makes the difference in driving forces for unwanted gases more negligible when compared to CO<sub>2</sub>. As a result, the purity of the permeate is higher, but the recovery % is lower as less CO<sub>2</sub> crosses at a low-stage cut. Decreasing the flow rate of the feed increases the amount of CO<sub>2</sub> that crosses but, in doing so, increases the driving force for other gases. Therefore, a higher stage cut leads to a lower purity but a higher recovery % of CO<sub>2</sub>. Membranes with higher areas lead to greater stage cuts, lower purity, and a higher % CO<sub>2</sub> recovery [12]. All of these parameters should be finely-tuned for m-DAC systems depending on the final goal, whether that be total recovery or a high purity for downstream applications.

In addition, these parameters may vary at each stage of a multi-step separation system. Energy requirements for installation, operation as well as manufacture of membranes must also be considered. Due to the infancy of m-DAC technology, there are very few parametric and gas module separation studies available. With that being said, several models that take these parameters into account have shown the scope of the possibility of m-DAC. High selectivity membrane material (HPM) with a CO<sub>2</sub> permeance of 2500 GPU and CO<sub>2</sub>/N<sub>2</sub> selectivity of 680 has been shown to be capable of a capture purity of nearly 20% in a single stage at a pressure ratio around 0.02, and commercial Polaris membranes (CO<sub>2</sub> permeance of 2000 GPU, CO<sub>2</sub>/N<sub>2</sub> selectivity of 30) can reach 50% with two stages [29]. HPM showed an exponential increase in CO<sub>2</sub> capture purity when decreasing the pressure ratio from 0.02, while no significant effect was observed for the Polaris membrane due to a negligible effect from concentration polarization [29]. For m-DAC, HPM and Polaris membranes required 3000 and 18,000 kWh/ton at one stage, respectively, to achieve 20 and 2.5% purity [29]. The study outlined the importance of a low-stage cut for improving the recovery ratio [29].



Although m-DAC CO<sub>2</sub> concentrations are not commonly tested, Lee et al. showed their ionic liquid + graphene oxide PIL-IL-GO facilitated transport membrane could produce a purity of 32% at 410 ppm CO<sub>2</sub> using only a single stage at 1 bar (1 bar = 100 kPa) of feed pressure [30]. Under these conditions, the membrane displayed a permeance of 3090 GPU and a CO<sub>2</sub>/N<sub>2</sub> selectivity of 1180 [30]. Unfortunately, the stage cut and pressure ratio were not reported. Proposed multistage membrane separation models have shown improved CO<sub>2</sub> separation with each stage and notably outline that the first stage has the highest energy, area, and emission values, after which each sequential stage shows an exponential decay [12].

Although very few papers have reported membrane separation under m-DAC conditions, the former examples indicate real promise and should encourage more widespread testing of membranes with atmospheric CO<sub>2</sub> capture in mind.

#### 4. Potential Membrane Materials

According to the concern above, the thickness of polymeric selective layers for DAC needs to be less than 1 μm. Hence, a typical membrane for DAC should consist of a thin selective layer deposited on an intermediate gutter layer on a porous substrate support, as shown in Figure 1. The gutter layer serves to protect from the penetration of the selective layer material into the porous support [25]. Highly permeable polydimethylsiloxane (PDMS) is frequently used as the gutter layer, and polyacrylonitrile (PAN) is used as the substrate [25,31–33]. Although each layer of material introduces transport resistance, the PDMS and PAN are so porous that their effect is negligible. Selective layers are manufactured by several different methods, including spin coating, dip coating, roll coating, blading, solution casting, dry-jet wet spinning (hollow fiber), and spray coating, with spin coating being the most common method for ultrathin membranes [32,34–37].

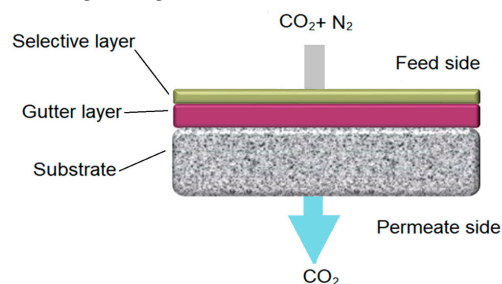


**Figure 1.** Sample diagram of typical gas separation membrane layers.

The selective layer is the most vital element of composite membranes and is modified with permeance and selectivity in mind. Fujikawa et al. recommend membranes with a CO<sub>2</sub> permeance of >10,000 GPU and CO<sub>2</sub>/N<sub>2</sub> selectivity of >30 for m-DAC. However, most current membranes fail to reach these specifications [12]. In the last decade, numerous promising polymeric membranes have stood out. Materials such as polymers of intrinsic microporosity (PIMs), polymers with ethylene oxide/ethylene glycol groups, mixed matrix membranes (MMMs), and facilitated transport membranes might meet the standards set by Fujikawa if their thickness falls below 1 μm as the permeance could be increased. Inorganic membranes have been explored in the past but often suffer drawbacks due to price and scalability [26].

In the last two decades, researchers have tried different approaches to increase permeability and selectivity, as well as to reduce the aging of membrane materials, for instance, introducing more rigid units into the polymer structure, post-modifying polymer structure with different functional groups, and adding functionalized nanofillers to membranes creating MMMs [38]. In this paper, we summarize the potential polymeric membrane materials for DAC. These materials with high permeability/permeance and/or high CO<sub>2</sub>/N<sub>2</sub> selectivity near or above the 2008 Robeson upper bound are mainly applied to CO<sub>2</sub> capture from point sources (Table 2). However, they could still be good starting candidates for further m-DAC development [39].

**Table 2.** Selection of recent promising membrane materials showing CO<sub>2</sub> permeabilities ≥ 1000 Barrer or with CO<sub>2</sub>/N<sub>2</sub> Selectivity's ≥ 30 at temperatures ≤ 35 °C. Inorganic membranes have not been included. Some additions are not mutually exclusive and could belong to several categories. Data is from pure gas permeation measurements. A more complete summary can be found in Table S1.

Polymeric Membranes		T (°C)	Pressure (kPa)	CO <sub>2</sub> Permeability (Barrer)	Gas Selectivity (CO <sub>2</sub> /N <sub>2</sub> )	Ref.			
Type	Polymers								
Polymer membranes	Copolymers	KAUST-PI-1	35	200	2389	33	[40]		
		PIM-BTrip (160 μm)	Aged 490 days	25	100	6060	31.0	[41]	
			Aged 120 days	25	100	6040	30.2	[41]	
		SFX-PIM-33 (Aged 130 days)	(Aged 130 days)	25	200	1848	30.8	[42]	
		BPM-50		35	350	4883	43	[43]	
		VAP7		30	100	1370	32	[44]	
		PTCNSi(OMe) <sub>3</sub>		20–22	100	2000	35.7	[45]	
		Polaris™ gen1		-	-	1000 (Commercially Available)	50	[46]	
		PolyActive™/85		-	-	1480	55	[47]	
		Copolymers with post modification	TZ-PIM-1		25	440	~3000	~30	[48]
			AO-PIM-1 + Methanol		35	200	1153	35	[49]
			MTZ100-PIM *		25	350	1391	22.2	[50]
			Thioamide-PIM-1 + Ethanol		25	100	1120	30.3	[51]
			cPIM-1		25	200	3739 ± 32	34.9	[52]
		Mixed matrix membranes	6FDA-durene/Si-5		25	200	3785	31	[53]
PIM-MFI3			25	100	2530	30	[54]		
Pebax-2533/ZIF	35 wt%		25	200	1287	32.3	[55]		
SPEEK/MIL-101 (Cr) 40 wt% *			30	100	30	40	[56]		
SPEEK/S-MIL-101 (Cr) 40 wt% *			30	100	35	41	[56]		
UiO-66-CN@sPIM-1 *			25	140	16,121.3	27	[57]		
PDMS-SAPO-34 (PM-30 wt%)			25	2000	5753	31	[58]		
PIM-1/GO			30	400	6169	123	[59]		
CNT-ZIF-8-PDMS			25	100	8705	45.6	[60]		
PAO-PIM-1/NH <sub>2</sub> -UiO-66	7 wt%		35	100	3825	30.0	[61]		
	0.5 wt%		35	100	~1400	~41	[62]		
PEO/HPNs	1 wt%	35	100	~1900	~44	[62]			
Facilitated transport membranes	Pebax [C4MIM][Gly] 20 wt%		25	100	~1100	~110	[63]		
	C(30)-P(1:1)		25	200	~1650	~55	[64]		
	Pebax-PEI-MCM-41-20		25	100	1521	102	[65]		
	15 wt% ([Cu(6)] <sub>2</sub> @13X)/6FDA-Durene		35	200	~1034	38.3	[66]		
	Pebax 1657/MWNTs-NH <sub>2</sub> /GTA (P10CN1G25)		35	700	1408	~40	[67]		
	Pebax 1657/SG 20 wt%		25	200	~1200	~55	[68]		
	CA/PM-4 (1:3 wt%)		35	300	3000	59	[69]		
	PIM-Py-Cl 15 wt%		25	200	4959.8	42	[70]		
	PIM-Py-Ac 15 wt%		25	200	6204.8	62	[70]		
PIM-Py-BF <sub>4</sub> 15 wt%		25	200	5584.3	46	[70]			

The membranes marked with a \* do not meet the table's criteria through pure gas testing but do meet the criteria under mixed gas conditions or humidified conditions which are covered later.

#### 4.1. Copolymers

Various copolymers with high CO<sub>2</sub> permeability and CO<sub>2</sub>/N<sub>2</sub> selectivity have been explored. Their structural designs focus on adding rigid structures to reduce interchain packing and create a microporous structure, in addition to frequently introducing ethylene oxide and ethylene glycol groups to enhance CO<sub>2</sub> affinity.

Aging is the major drawback of these microporous polymers [38,71]. Aging refers to the thermodynamic stabilization of the membrane polymer packing, which leads to a collapse of pores and a loss of free volume, resulting in a decrease in permeability. This phenomenon is observed after short periods of time and at accelerated rates with thinner membranes [25,34,72,73]. Membranes also suffer from plasticization, where CO<sub>2</sub> sorption at high pressures increases polymer chain movement. This leads to an increased permeability for all gasses due to an increase in free volume and, consequently, a decrease in selectivity [74].

Introducing rigid and bulky units into the polymer chain can efficiently increase CO<sub>2</sub> permeabilities with or without aging while still maintaining moderate selectivity due to their special chain rigidity. PIMs are a good example of polymers that successfully increase permeability by introducing rigid structures into the polymer chain. PIMs are usually composed of two components: (i) a structural unit that possesses concavities and introduces a site of contortion into the polymer chain and (ii) a linking group (e.g., derived from dibenzodioxin or imide formation) that fuses the structural units together during polymerization and leads to inefficient packing and high free volume [25,73,75]. Some of these polymers offer high permeability as well as cheap facile manufacture. The main building blocks of PIMs are (i) spirobisindane (SBI); (ii) phenazine; (iii) ethanoanthracene (EA); (iv) triptycene (Trip); (v) benzotriptycene (BTrip); (vi) spirobifluorene (SBF); (vii) Tröger's base (TB); and (viii) tetraphenylethylene etc. [76]. Polyimides of intrinsic microporosity (PIM-PIs) can also be prepared when structural PIM motifs containing rigid and bulky contortion sites are introduced into polyimide backbones. The structural design can be manipulated in many different ways depending on the location of the contortion site, for example, either in dianhydride or diamine monomers for PIMs-PIs. The method in which PIMs are synthesized has been shown to have an effect on chain packing, membrane structure, performance, and aging.

PIMs containing Trip and BTrip (Figure 2a) units exhibit excellent CO<sub>2</sub> permeabilities (up to ~22,000 Barrer) [41]. Their highly rigid structure leads to observed ultramicroporosity, which facilitates the transport of smaller gas molecules whilst increasing the activation energy for larger molecules like N<sub>2</sub>. Experimentally, PIM-BTrip has been shown to have a high diffusivity, leading to greater permeability whilst maintaining selectivity due to the selective molecular sieving based on kinetic diameter [41]. KAUST-PI-1 is another example of a co-polymer that boasts high permeability due to its rigid backbone structure, which effectively leads to the formation of ultra-porous structures (Figure 2b). It was also observed that the choice of bridgehead group had a significant effect on the permeability of KAUST-PI-1. The bulky isopropyl bridgeheads and methyl-substituted diamines increased intrachain rigidity and improved CO<sub>2</sub> permeability 4-fold [40]. Co-polymer designs with bulky groups in mind, like SFX-PIMs (Figure 2c), have shown CO<sub>2</sub> permeabilities comparable to the PIM-1 standard but with improved CO<sub>2</sub>/N<sub>2</sub> selectivity around 30 [42]. PIM-bpy-x gas separation performance was enhanced by incorporating bulky structures into the polymer through the polycondensation of a tetraphenyl bipyrimidine monomer (Figure 2d). PIM-bpy-x exhibited excellent gas separation performance (4234 barrer)—a 21% improvement in CO<sub>2</sub> permeability. The increase in CO<sub>2</sub> permeability is due to the affinity of the N-rich bipyrimidine units for CO<sub>2</sub> [77].



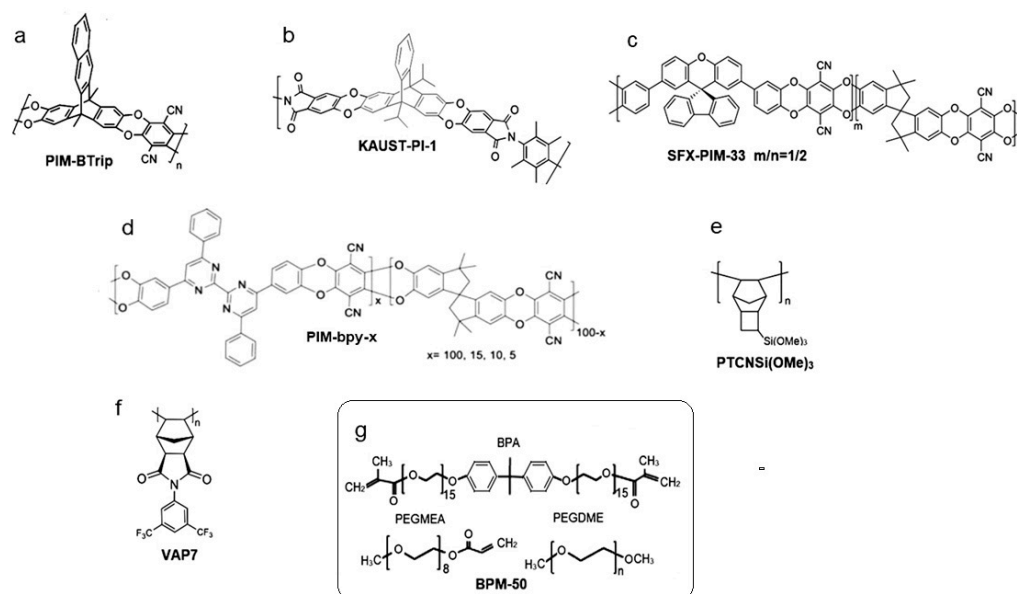


**Figure 2.** Chemical structures of high permeable copolymers, with  $\text{CO}_2$  permeabilities  $\geq 1000$  Barrer or with  $\text{CO}_2/\text{N}_2$  Selectivity's  $\geq 30$  at temperatures  $\leq 35$  °C. (a) PIM-BTrip [41], (b) KAUST-PI-1 [40], (c) SFX-PIM-33 ( $m/n = 1/2$ ) [42], (d) PIM-bpy- $x$  [77], (e) PTCNSi(OMe) $_3$  [45], (f) VAP7 [44], (g) BPM-50 [43].

High permeable polymers synthesized from different modified monomers have also shown the improvement of gas separation properties. Grazia Bezzu et al. conducted a combined simulation and experimental study to investigate the effect on polymer microporosity and gas permeability of PIM-SBFs by placing simple substituents such as methyl, *t*-butyl, and fused benzo groups onto spirobifluorene monomers. It was shown that methyl or *t*-butyl substituents both cause a large increase in gas permeabilities, with four methyl groups enhancing the concentration of ultramicropores ( $<0.7$  nm), which contribute to selective gas transport. The *t*-butyl substituents lower selectivity by generating a greater concentration of larger, less selective micropores ( $>1.0$  nm) due to their size [78]. Alentiev et al. wonderfully demonstrated the variability that can occur with subtle modifications of side groups on the monomers (Figure 2e). Following this strategy of monomer substituent modification, new high molecular weight metathesis and addition polynorbornenes with (AlkO) $_3$ Si-groups of different lengths (Alk = Me, Et, *n*-Pr, *n*-Bu) were synthesized. These polymers, with similar scaffolding, consist of two parts—glassy (rigid polymer main chains) and rubbery (flexible side chains), which allowed dramatic tuning of polymer properties by the modification of polymer main chain structures and the length of trialkoxysilyl side groups. PTCNSi(OMe) $_3$ , for example, showed a selectivity of 35.7 while increasing the length of substituents with PTCNSi(OEt) $_3$  led to a selectivity drop down to 21.3 [45]. The drop in selectivity was likely due to the longer chains creating larger pores. Nazarov et al. performed a similar study exploring several modified monomers that formed vinyl-addition polymers. VAP7 was the most promising for DAC application (Figure 2f). VAP7's performance can be attributed to the trifluoromethyl groups, which hinder inter-chain interactions, leading to an increase in free volume due to a decrease in favorable chain packing [44].

Ethylene oxide and ethylene glycol groups have been exploited in membrane design due to their high affinity for  $\text{CO}_2$  by Lewis base interactions, which often lead to a higher selectivity for  $\text{CO}_2$  [79,80]. Membranes are not made solely of polyethylene glycol due to the high crystallinity induced by strong hydrogen bonding, which is not attractive for gas permeability. Both Polaris and Polyactive (shown in Table 2) are commercial copolymers containing PEO groups [80,81]. Both of these PEO-containing copolymers show  $\text{CO}_2/\text{N}_2$  selectivity over 30 and respectable  $\text{CO}_2$  permeance [46,47]. Pebax 1657 is also a promising PEO-containing commercial polymer that is frequently used in MMM

applications. BPM-50 (Figure 2g), an oxygen-containing copolymer that was formed through the UV polymerization of PEGMEA, BPA, and PEGDME, boasts an impressive CO<sub>2</sub> permeability of 4883 Barrer and CO<sub>2</sub>/N<sub>2</sub> selectivity of 43. In addition, the method of preparation for BPM-50 is clean, rapid, and solvent-free [43].

Another effective approach to significantly improving the permeability and selectivity is post-modifying copolymers. The functionalization of promising copolymers allows for further enhancements to gas separation performance (Table 2). Taking TZPIM as an example (Figure 3a), the tetrazole structures from the modification of nitrile groups in PIM-1 raise the affinity for CO<sub>2</sub>, hence increasing the single gas selectivity of CO<sub>2</sub>/N<sub>2</sub> to 30. These tetrazole groups also serve to increase rigidity through hydrogen bonding, which in turn increases plasticization resistance from CO<sub>2</sub> [48]. Further modifying TZPIM to MTZ100-PIM (Figure 3b) increases solvent processability over TZPIM-1, which is of critical importance for large-scale membrane fabrication [50]. MTZ100-PIM showed a significant change in performance between pure and mixed gas permeation testing. Under pure gas testing, MTZ100-PIM showed a CO<sub>2</sub> permeability of 1391 barrer and a CO<sub>2</sub>/N<sub>2</sub> selectivity of 22.2. Conversely, mixed gas testing with a 2:8 CO<sub>2</sub>:N<sub>2</sub> per volume mixture yielded more impressive results with a CO<sub>2</sub> permeability 2057 barrer and a CO<sub>2</sub>/N<sub>2</sub> selectivity of 41.6. This behavior is attributed to a suppression of N<sub>2</sub> permeability as condensable CO<sub>2</sub> occupies sorption sites far more than the non-condensable N<sub>2</sub>, reducing the rate of passage for N<sub>2</sub>. AO-PIM-1 is an excellent example of the common observations that come with functionalization (Figure 3c). The oxygen and nitrogen groups lead to more interchain interactions, which causes a net decrease in microporosity and the formation of more narrow pores. This, in turn, results in a decrease in CO<sub>2</sub> permeability and an increase in CO<sub>2</sub>/N<sub>2</sub> selectivity to 35 due to the electronegative groups interacting favorably with CO<sub>2</sub> [49]. Thioamide-PIM (Figure 3d) continues this trend with lower CO<sub>2</sub> permeability but higher CO<sub>2</sub>/N<sub>2</sub> selectivity (30.3) when compared to PIM-1 [51]. Yu et al. recently tested di-substituted PIM-1 (D-cPIM-1) and branched PIM-1 (B-cPIM-1) containing carboxylic acid groups (Figure 3e). They found that the 70% hydrolyzed di-substituted PIM-1 showed a CO<sub>2</sub> permeance of 7700 GPU and CO<sub>2</sub>/N<sub>2</sub> selectivity of 56. More importantly, although the branched hydrolyzed PIM showed a lower CO<sub>2</sub> permeance of 3200 GPU, it showed no decrease in permeance after 60 days, indicating the branched structure may be vital for aging resistance [71]. These hydrolyzed PIMs have also been investigated for increasing CO<sub>2</sub> permeability due to quadrupole interactions, as further illustrated by cPIM-1 [52].

PIM and several polymers with similar structures are often treated with ethanol or methanol to remove residual solvent from casting and increase the diffusion coefficient, thus increasing permeability [82,83]. UV treatment has also been shown to increase performance due to chain scission and oxidation of the polymers [84].

Although the CO<sub>2</sub>/N<sub>2</sub> gas separation performance of some polymers synthesized via thermal or UV treatment meets our summary criteria showing increased separation properties, e.g., carbon molecular sieves, TOX-PIM-1 [85], PIM-300 [86], and PIM-1-UV/Ozone [84], the high fabrication temperature, brittleness of thin sheets and poor solubility after treatment could limit their feasibility in m-DAC.

#### 4.2. MMMs

The introduction of filler materials into polymeric membranes integrates their advantageous properties and provides a feasible approach to fabricating membranes for DAC [87–89]. These fillers offer a wide range of functionality due to their varying structures and often have low cost. Most added fillers help with molecular sieving due to their innate structure or, based on their dispersion/interaction with the polymeric material, can help create free volume and improve the gas-membrane affinity to provide effective solutions for overcoming the performance trade-off effect [57]. These structures can range from 0D to 3D with varying complexities and molecular interactions with gas molecules [90].

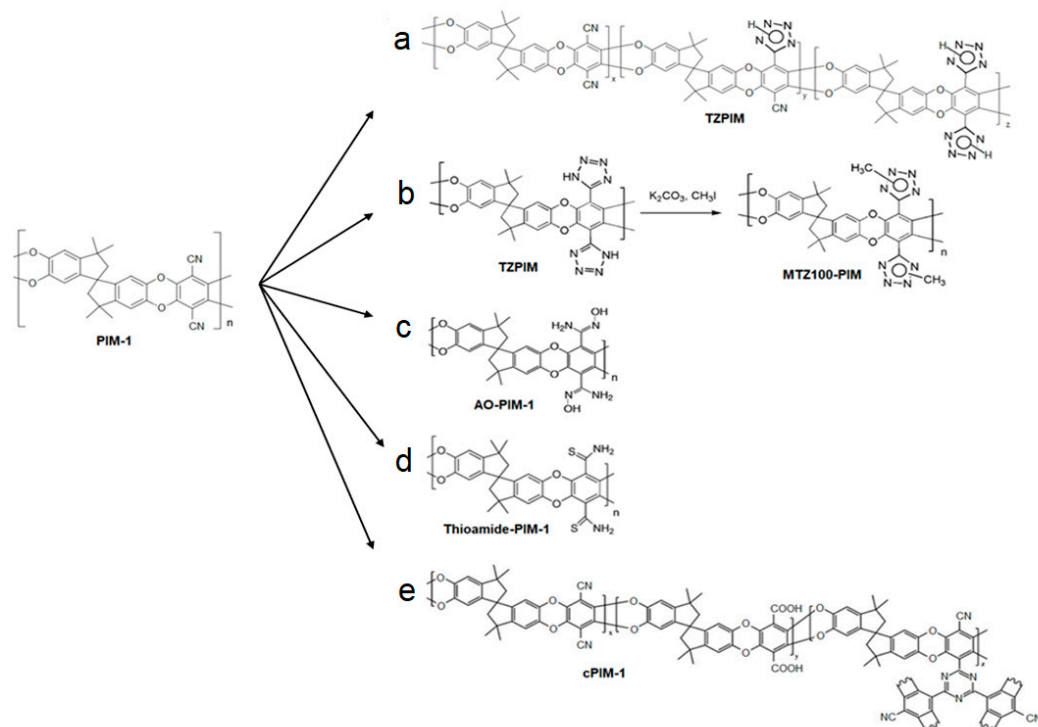


**Figure 3.** Chemical structures of copolymers with post modification ( $\text{CO}_2$  permeabilities  $\geq 1000$  Barrer or with  $\text{CO}_2/\text{N}_2$  selectivity's  $\geq 30$  at temperatures  $\leq 35$  °C). (a) TZPIM [48], (b) MTZ100-PIM [50], (c) AO-PIM-1 [49], (d) Thioamide-PIM-1 [51], (e) cPIM-1 [71].

Amongst the crowd of MMM fillers, MOFs stand out as they consistently have positive effects on membrane performance depending on their loading [57,91–93]. For example, UiO-66-CN covalently linked with s-PIM boasted a  $\text{CO}_2$  permeability of 16,121 Barrer and  $\text{CO}_2/\text{N}_2$  single gas selectivity of 27.0. In addition, when tested under 1:1  $\text{CO}_2:\text{N}_2$  by volume, the selectivity increased to 53.5 (Figure 4a). This is explained by the high porosity and rich sorption sites in the 3-D MOF domain, where  $\text{CO}_2$  is competitively adsorbed over  $\text{N}_2$  [57]. UiO66- $\text{NH}_2$  doped with  $\text{Ag}^+$  leads to great increases in gas separation characteristics when tested under 1:9  $\text{CO}_2:\text{N}_2$  by volume as  $\text{Ag}^+$  raises the hydrophilicity and facilitates  $\text{CO}_2$  transport while also leading to an increase in free volume, which characteristically increases permeability to  $>15,000$  Barrer with selectivity 30 [94]. Wang et al. reported a hybrid membrane containing UiO66- $\text{NH}_2$  in PAO-PIM (Figure 4b). The amidoxime and amine groups tend to form hydrogen bonds, creating a hydrogen bond network between the two phases, which raised the  $\text{CO}_2$  permeability from 2902 to 3825 Barrer due to an increase in the diffusivity coefficient while still maintaining a respectable selectivity [61].

3D MOF fillers are not the only inorganic fillers being explored for mixed matrix membranes. The addition of silica nanoparticles is an efficient strategy for boosting the initial gas permeability and suppressing physical aging. By incorporating 0.05 wt% sulfonic acid-functionalized silica nanosheets (S-SN) into the PIM-1 polymer, the resulting membrane showed a 40% higher  $\text{CO}_2$  permeability and 22% enhancement in  $\text{CO}_2/\text{N}_2$  selectivity. 150-day-aged freestanding PIM/SN1 and 28-days-aged TFN PIM/S-SN0.05 showed 70% and 5 times greater  $\text{CO}_2$  permeability than the pure thick PIM-1 and TFC PIM-1 membranes, respectively [35] (Figure 4c). Similarly, Nafisi et al. studied the effect of silica nanoparticle loading in both Pebax and 6FDA-durene matrices. They found that the integration of silica nanoparticles raised the permeability in both cases, more dramatically with 6FDA durene (Figure 4d). They observed an increase in Fractional Free Volume (FFV) with filler loading; FFV increases as the density of the membrane decreases. The more drastic increase in permeability observed with 6FDA durene is hypothesized to be due to its glassy nature; therefore, the presence of nanoparticles has a greater effect on the FFV [53].

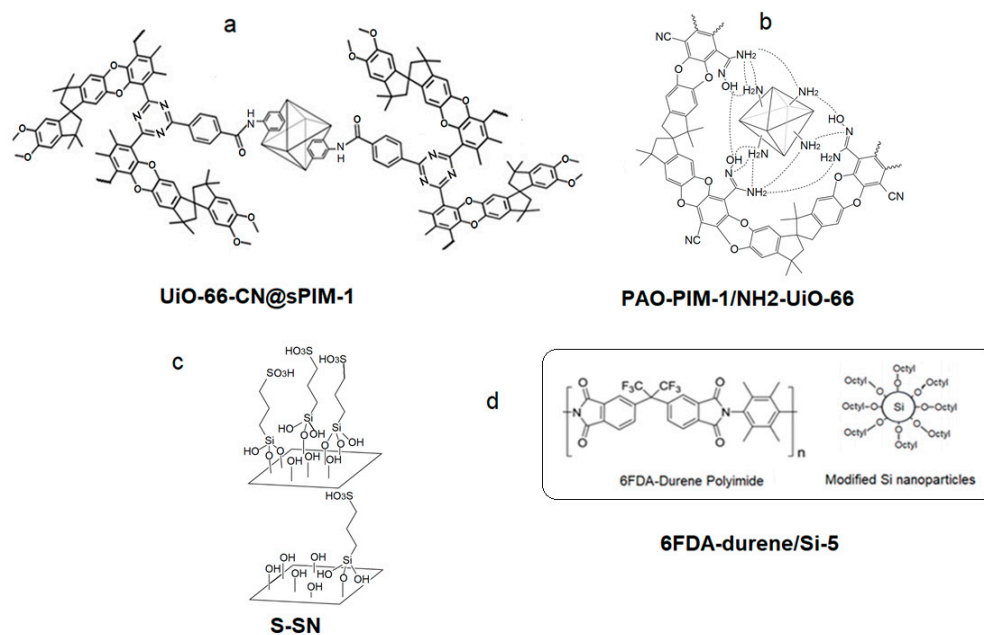


**Figure 4.** Examples of high permeable MMMs with MOF and Silica nanoparticles ( $\text{CO}_2$  permeabilities  $\geq 1000$  Barrer or with  $\text{CO}_2/\text{N}_2$  Selectivity's  $\geq 30$  at temperatures  $\leq 35$  °C). (a) UiO-66-CN@sPIM-1 [57], (b) PAO-PIM-1/ $\text{NH}_2$ -UiO-66 [61], (c) S-SN [95], (d) 6FDA-durene/Si-5 [53].

Other inorganic fillers, such as synthetic zeolite—SAPO-34, can also largely increase the  $\text{CO}_2$  permeability of MMMs [95]. Similarly, SAPO-34 raises the free volume of polymer membranes, leading to an increase in permeability and raising selectivity when selectively sieving molecules based on kinetic diameter [58]. It was reported that a PDMS-SAPO-34 (PM-30 wt%) membrane exhibited a  $\text{CO}_2$  permeability of 5753 Barrer with an ideal  $\text{CO}_2/\text{N}_2$  selectivity of about 31 at 2000 kPa (20 bar) and 25 °C, which surpassed the 2008 Robeson upper bound for  $\text{CO}_2/\text{N}_2$  separation.

Also, a large number of novel inorganic fillers could not only help tune the free volume of the polymer matrix but also create the coefficient path. Carbon nanotubes and graphene oxide (GO) nanosheets are examples of such fillers. Efficient  $\text{CO}_2$  transport pathways were constructed by the homogeneous dispersion of carbon nanotubes (CNTs) and GO within MMMs, leading to both enhanced permeability and selectivity. Li et al. showed that mixing both carbon nanotubes and GO fillers into Matrimid membranes displayed a synergistic relationship [96]. The extraordinarily smooth walls of CNTs acted as a highway for high permeability, whereas the graphene oxide nanosheets acted as a selective barrier to create a more tortuous diffusion pathway for  $\text{N}_2$ , meanwhile providing a more selective path for  $\text{CO}_2$  through interactions with the hydroxyl and carboxyl groups on the GO surface (Figure 5). The membrane combining 5 wt% of CNTs and 5 wt% of GO (Matrimid<sup>®</sup>-CNTs/GO-5/5) displayed optimum performance with a  $\text{CO}_2$  permeability of 38.07 Barrer, a  $\text{CO}_2/\text{N}_2$  selectivity of 81.00. Compared to pure Matrimid<sup>®</sup> membranes, the  $\text{CO}_2$  permeability and  $\text{CO}_2/\text{N}_2$  selectivity of the Matrimid<sup>®</sup>-CNTs/GO-5/5 membranes were increased by 331% and 147%, respectively. Although the reported 38.07 Barrer is still much lower than the expected permeability of  $\text{CO}_2$  for m-DAC, the method inspires future research on designing high-performance membranes for DAC. More effort needs to be put into choosing the proper polymer matrix. Furthermore, to achieve high performance, ideal polymer–filler interface morphology and homogenous filler dispersion have to be realized. These challenges can be addressed by appropriate screening or modification of fillers to balance the polymer–filler, and filler–filler interactions [97].



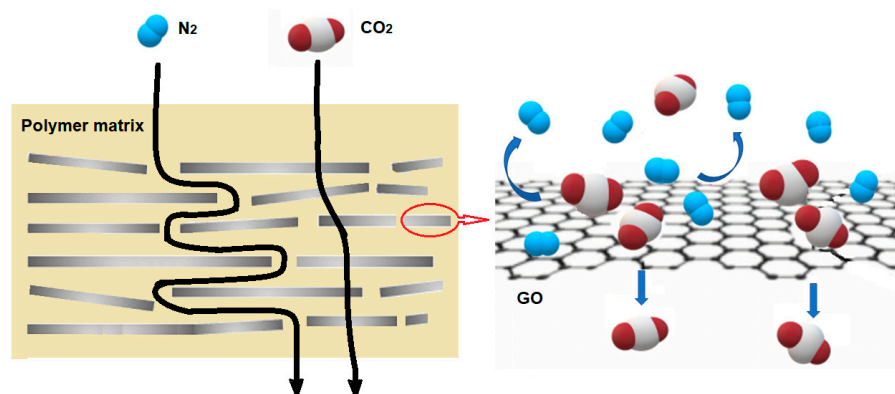


**Figure 5.** Schematic of the mechanism for gas travel through MMMs with GO fillers.

Besides inorganic fillers, organic hollow nanoparticles have great promise for creating new highly permeable membranes. Ding et al. fabricated hollow polyamide nanoparticles (HPN) with a dense shell via interfacial polymerization in a surfactant-free microemulsion. The hollow nanoparticles combined with liquid acrylate monomers to form mixed matrix membranes via UV-induced photo-polymerization. The nanoparticles with an average diameter of 42 nm dispersed uniformly in the membranes. The  $\text{CO}_2$  permeability and  $\text{CO}_2/\text{N}_2$  permselectivity of the MMMs both increased as the nanofiller loading increased. The gas permeation and separation performance exceeded the Robeson upper bound line with a maximum  $\text{CO}_2$  permeability of 1898 Barrer and a maximum  $\text{CO}_2/\text{N}_2$  permselectivity of 43.9 at 1 wt% nanofiller loading. The improvement mainly arose from the increase in the  $\text{CO}_2$  solubility, the  $\text{N}_2$  diffusivity, and the  $\text{CO}_2/\text{N}_2$  solubility selectivity [62].

In addition, several novel molecular-scale fabrication methods render highly efficient polymeric composites and could be potentially applied for m-DAC. Instead of using traditional substrates and gutter layers, Ashtiani et al. developed membranes with carbon nanotube support structures and a ZIF-8 gutter layer (zeolitic imidazolate frameworks-ZIF). The surface was spray-coated with PDMS, which helped fill any gaps or interfacial defects. Due to the ZIF-8's metal sites,  $\text{CO}_2$  was effectively permeated through feeble electrostatic fields and the quadrupole moments of  $\text{CO}_2$  [60]. The in-situ micelle-induced blending approach is another significant step toward realizing high-performance  $\text{CO}_2$  separation membranes. Seong et al. reported highly  $\text{CO}_2$ -permeable membranes obtained by blending in situ self-assembled micellar-structured poly(poly(ethylene glycol) methyl ether acrylate) (PPEGMEA) with poly(ether-block-amide) (Pebax) (Figure 6). The Pebax/PPEGMEA (30/70 *w/w*) blend membrane comprised highly  $\text{CO}_2$ -philic PPEGMEA micelles, which appreciably increased the d-spacing of the Pebax matrix. Consequently, the blend membrane containing a high molecular weight of PPEGMEA exhibited an unprecedented  $\text{CO}_2$  permeability enhancement of 1054% compared to the pristine Pebax membrane while maintaining good  $\text{CO}_2$  selectivity relative to  $\text{N}_2$  because of the enriched polyethylene glycol moieties. This excellent separation performance was maintained for 100 h up to 10 atm, validating the good long-term separation performance of the membrane [98]. Furthermore, the membrane exhibited good mechanical strength and plasticization tolerance. Similarly, membranes formed through the radical polymerization of PEGMEA, PEGDA, and PEGDME presented  $\text{CO}_2$  permeability of 2980 Barrer and  $\text{CO}_2/\text{N}_2$  selectivity of 45.7 with stability over 500 h [99]. Gel mixed matrix composites provide a class of membranes with high  $\text{CO}_2$  permeability and stability performance. The fillers incorporate alongside small molecule liquid substances to increase free volume [100]. Chen et al. prepared EM400/MIL-101(Cr)- $\text{NH}_2$  MMMs; the addition of MIL-101(Cr)- $\text{NH}_2$  improved the mechanical properties of the membrane and increased the selectivity of  $\text{CO}_2/\text{N}_2$ . The EM400/MIL-101(Cr)- $\text{NH}_2$  MMMs were further modified with tripropionin. The tripropionin greatly improved the  $\text{CO}_2/\text{N}_2$  separation performance of the g-MMMs by increasing the FFV and the  $\text{CO}_2$  solubility coefficients at the same time. The  $\text{CO}_2$  permeability was increased from 213 to 1182 Bar-



rer when compared to the EM400/MIL-101(Cr)-NH<sub>2</sub> MMMs without TPP. This kind of gel-MMM also showed stability over 168 h of aging testing [100]. An alternative study tested SPEEK/MIL-101 (Cr) and SPEEK/S-MIL-101 (Cr) membranes at 40% loading under humidified conditions. Under these conditions, both membranes showed permeability improvements from 30 to 1623 Barrer and 35 to 2064 Barrer, respectively. Although the selectivity for SPEEK/MIL-101 (Cr) membranes did not change from 40, the selectivity did improve from 41 to 53 in the case of SPEEK/S-MIL-101 (Cr). The proportionality between permeability and water content was attributed to an increase in pore swelling, while the increase in selectivity can be explained by the decreased level of transport resistance for CO<sub>2</sub> with water as compared to N<sub>2</sub> [56].

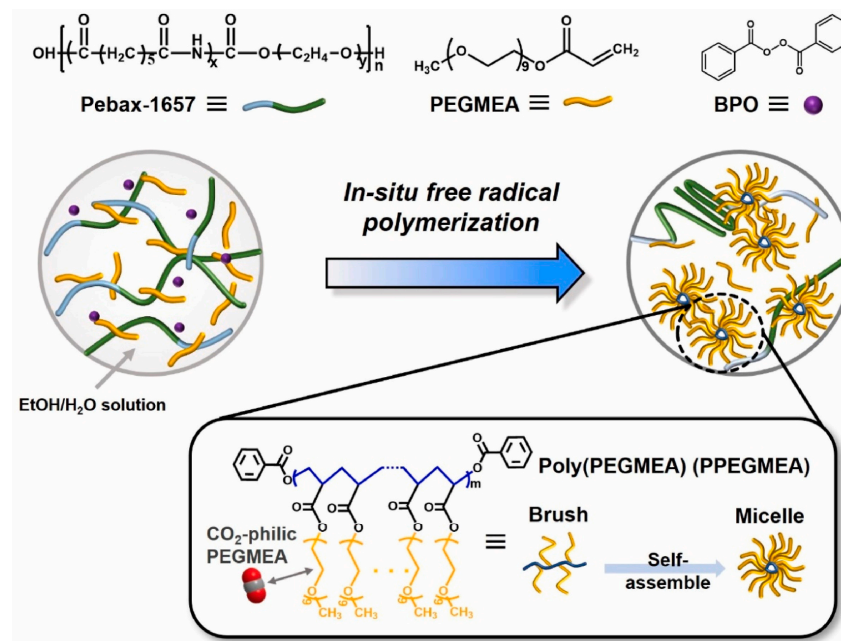


**Figure 6.** Schematic of Pebax/PPEGMEA membranes obtained via the free radical polymerization of PEGMEA in Pebax in the presence of BPO. Reprinted with permission from Ref. [99]. Copyright 2022 Elsevier.

#### 4.3. Facilitated Transport Membranes

Finally, facilitated transport membranes are unique in their exceptionally high selectivity for CO<sub>2</sub> compared to typical solubility/diffusion membranes due to reversible reactions between the carriers in the membrane and CO<sub>2</sub>. The carriers can be divided into fixed or mobile carriers (Figure 7). These reversible reactions require water to occur, setting a dependence on the humidity of the feed gas [101]. When considering m-DAC, the need for humidity can lead to tighter requirements for installation limited to humid areas or introduce higher operating costs and water requirements for humidifying the feed gas. With that being said, PIL-IL-GO membranes have been tested under m-DAC conditions of 410 ppm CO<sub>2</sub> and showed CO<sub>2</sub> permeances between 3000 and 4000 GPU with very high CO<sub>2</sub>/N<sub>2</sub> selectivity (>1000) [30]. There are various carrier structures, but most are based on amines. For example, P(DADMACA-co-VAm) membranes containing primary amino groups, carbonate groups, and quaternary ammonium groups show synergistic increases in membrane separation performance over their homogeneous counterparts (PVAm/PDADMACA) with a CO<sub>2</sub> permeance of 1842 GPU and a CO<sub>2</sub>/N<sub>2</sub> selectivity of 160 [63]. In addition, PVA membranes have been modified with both SiO<sub>2</sub> nanofillers and [bmim][Tf<sub>2</sub>N] ionic liquid to produce membranes with a CO<sub>2</sub> permeance of 3016 GPU and a CO<sub>2</sub>/N<sub>2</sub> selectivity of 62 [102]. The use of ionic liquids may not be the best practice as they can be high-cost and harmful to the environment and living organisms, therefore eliminating one of the advantages of m-DAC over the other sorption technologies [103].

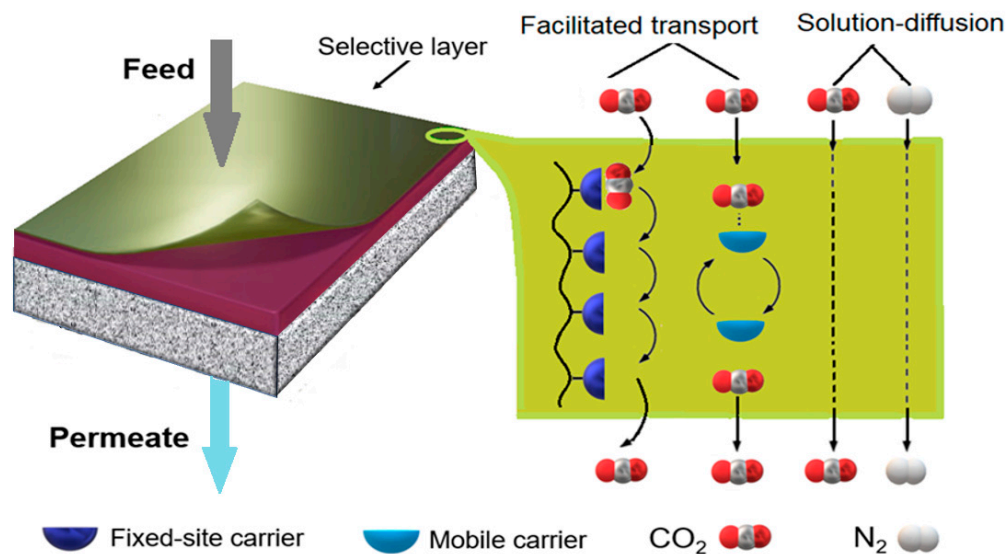
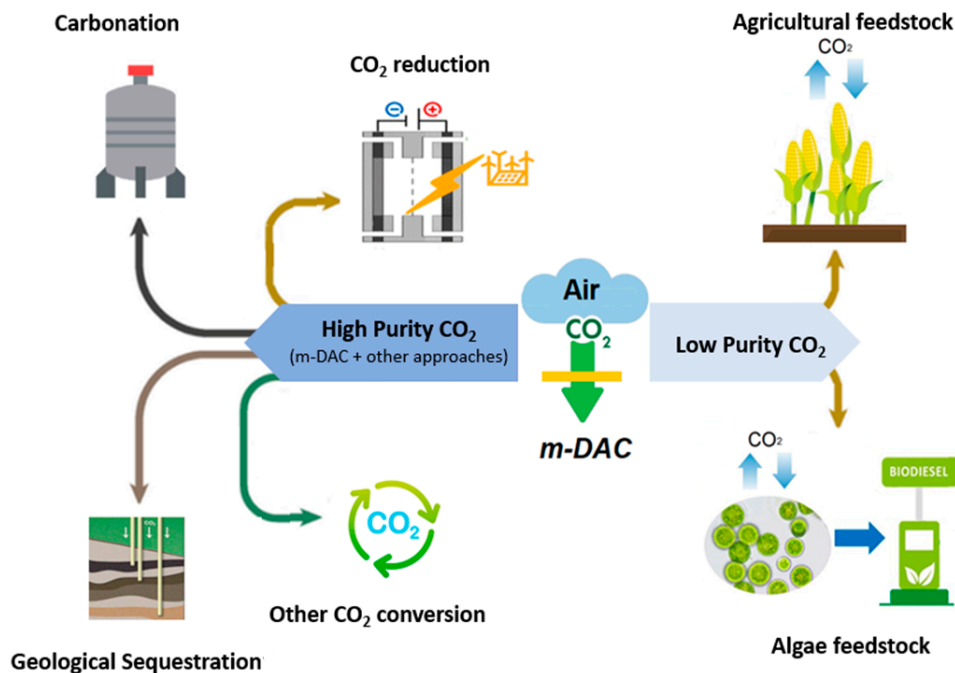


Figure 7. CO<sub>2</sub>/N<sub>2</sub> separation through the facilitated transport membrane [12,104].

### 5. M-DAC Application

Once CO<sub>2</sub> is captured by DAC, it can be stored or recycled for use in several different downstream applications, as summarized in Figure 8. One important parameter for any CO<sub>2</sub> utilization after capture is the percent purity of CO<sub>2</sub>. The most common method of CO<sub>2</sub> storage is geological sequestration; generally, geological storage of CO<sub>2</sub> requires CO<sub>2</sub> gas at a high purity (more than 98%) [5,105]. Currently, a purity over 90% is not possible to achieve by m-DAC efficiently in 1 stage; therefore, geological storage is an unlikely application of m-DAC without several stages or pairing with other CO<sub>2</sub> capture approaches [5,12,16]. A simulation-based study using a membrane with a CO<sub>2</sub> permeance of 1850 GPU and CO<sub>2</sub>/N<sub>2</sub> selectivity of 80 for hybrid membrane cryogenic (HMC) capture showed a 9% reduction in capture cost at a capture ratio of 85% compared to conventional monoethanolamide (MEA) carbon capture [106,107]. Similarly, another HMC process using a membrane with a CO<sub>2</sub> permeance of 1000 GPU and CO<sub>2</sub>/N<sub>2</sub> selectivity of 100 was shown to reduce the energy requirement compared to MEA capture from 4.409 GJ<sub>th</sub>/tCO<sub>2</sub> to 3.25 GJ<sub>th</sub>/tCO<sub>2</sub> from a stream of 15% CO<sub>2</sub> and a pressure ratio of 11.11 achieving a capture ratio of 85% and a purity over 89% [107,108]. Unfortunately, there is a lack of research on hybrid separation systems using membranes alongside other DAC methods, which have the possibility for efficient cost reductions. A recent engineering parametric study, which investigated the impact of material performance, process design, and operating conditions on membrane-based DAC, shed light on the future of this technique. The study concluded that with existing commercial membrane materials, the maximal CO<sub>2</sub> output concentration from a single-stage separation would be ~2%. A similar two-stage process could increase this to ~50%, noting that O<sub>2</sub> and water would be co-permeated. High-performance materials (not commercialized) could achieve ~12% in a single stage and up to ~99% in two stages [16]. For these high-performance materials in a two-stage process, costs and energy fall in the affordable range, e.g., 103 to 104\$ per tCO<sub>2</sub> with a first-order optimized energy requirement of 101 GJ per tCO<sub>2</sub> [16]. Currently, multi-stage membrane modules are still needed if high-purity outputs are desired since the performance might worsen due to pressure drop and concentration polarization [16]. Hence, it could be an efficient approach to produce high-concentration CO<sub>2</sub> via a hybrid system, which combines m-DAC and other CO<sub>2</sub> capture systems, although more research is needed in this area.



**Figure 8.** Examples of post-capture utilization pathways for CO<sub>2</sub> depending on purity.

With m-DAC, the contaminants impacting CO<sub>2</sub> purity are gases like O<sub>2</sub> and N<sub>2</sub>, not NO<sub>x</sub> and SO<sub>x</sub>, which are picked up by flue gas capture. It seems only agricultural applications can use dilute CO<sub>2</sub> [5]. Biological fixation through photosynthetic organisms is the planet's natural method for CO<sub>2</sub> recycling; photosynthetic microorganisms offer fast reproduction, adaptability, and efficient conversion of CO<sub>2</sub> into sugars and typically require low CO<sub>2</sub> (<~40%) concentrations [16,109] (Table S2). With currently commercially available membranes, the 2% CO<sub>2</sub> concentration could be of interest for the intensification of greenhouses or algae ponds. Captured high-purity CO<sub>2</sub> can also be used to enhance oil recovery. It can be used for welding, dry ice, soda, and feedstock for greenhouses and other agricultural installations. Furthermore, CO<sub>2</sub> can be used for conversion to several commercial chemicals such as ammonia for fertilizer, plastics which reduce the use of petrochemical products, formic acid, synthetic fuels by methanation, and methanol, to name a few [109]. In that event, multistage membrane units or hybrid processes could be of interest [29]. Although most electrochemical reduction of CO<sub>2</sub> uses pure CO<sub>2</sub>, recent studies have shown that CO<sub>2</sub> reduction to CO can be achieved with low CO<sub>2</sub> purity, indicating another realistic use for m-DAC CO<sub>2</sub> [110]. The CO produced can be used to produce useful hydrocarbons for downstream applications. For all the aforementioned uses, the source of energy (renewable or not) for conversion and the processes' emissions should be considered to determine the overall environmental impact and the extent of negative emissions.

Currently, since m-DAC is rather expensive with current membranes, the most attractive selling point is the modularity. Fujikawa et al. showed through process simulation that a 4-stage separation module using current highly permeable membranes can fit into 0.01 m<sup>3</sup> and capture 1 kg-CO<sub>2</sub> per day [12]. Dittmeyer et al. proposed DAC-integrated AC units that could convert captured CO<sub>2</sub> into hydrocarbon fuels. Their paper provided perspective examples of towns fueling their cars using the fuels generated by negative emission technologies. This approach could add an incentive for the public to get involved in DAC technology [25]. Small-scale m-DAC installations have the potential to be installed in office buildings and schools where the CO<sub>2</sub> concentration reaches up to 1000 ppm [34]. Areas with elevated CO<sub>2</sub> concentrations compared to the atmosphere would increase the capture efficiency of m-DAC. Moreover, the location independence of m-DAC allows for installation near CO<sub>2</sub> storage and recycling sites. This process can avoid the construction of pipelines needed to transport the CO<sub>2</sub> recovered from location-dependent capture sites to

storage sites [7]. This also avoids the energy required to compress the gas for transport. Using the previously mentioned utilization of CO<sub>2</sub> as an agricultural feedstock as an example, m-DAC modules could become a standard installation in every greenhouse.

## 6. Perspective

The m-DAC process has been highlighted as a promising complementary technology to sorbent-based DAC. Currently, the major barriers facing m-DAC's full-scale implementation include membrane material performance, membrane fabrication, and system process development [12]:

### (1) Membrane materials

The performance of membrane materials is significantly affected by the trade-off of permeance/selectivity as well as plasticization and physical aging. More research needs to be conducted on m-DAC materials to meet the criteria of CO<sub>2</sub> permeance > 10,000 GPU and CO<sub>2</sub>/N<sub>2</sub> selectivity > 30. Manipulation of the physical (mainly free volume) and chemical (mainly reactivity with CO<sub>2</sub>) membrane environment to improve performance via novel chemistries and preparative methods should continue to be an active area of research [86]. Besides employing novel chemistries to prepare polymers via improving the chain rigidity by introducing more inflexible units, the development of polymer nanocomposites through different approaches, e.g., "in-situ micelle-induced blending" and "gel mixed matrix compositing". Additionally, using proper nanomaterials, such as selected functionalized MOF, silica, and GO, looks promising in terms of CO<sub>2</sub>/N<sub>2</sub> separation performance, cost, synthesis, and feasibility. Notably, some inorganic/organic fillers could not only help tune the free volume of the polymer matrix but also increase CO<sub>2</sub> solubility or create a coefficient path [98].

In addition, exploiting facilitated transport mechanisms can also provide effective solutions for overcoming the performance trade-off effect [57]. Low-cost and high-performance membranes for DAC are required by industry. Hence the exploration of cheaper and affordable materials should always be pursued.

### (2) Membrane fabrication

To meet the performance expectation of DAC and be employed in large-scale applications, membrane materials should be capable of forming thin membranes with selective layers less than 1 μm to enable high gas permeance and be packaged into large spiral wound or hollow fiber membrane modules to maximize the surface area to volume ratio [46]. In this sense, the nanofillers for mixed matrix membranes need to be carefully chosen and appropriately dispersed. Polymers that are not solvent-processable or prepared at high temperatures should attract less attention. It seems that commercially available Pebax (PEO-based polymers) and PVAm-based facilitated transport membranes are good candidates for selective coating layers [64,79].

### (3) System and process

Improvements to the process durability of m-DAC systems against the typical, high TRL (Technology Readiness Level) separation operations, such as adsorption, absorption, and cryogenic distillation, should be made. Compared to CO<sub>2</sub> separation from point sources, rather than impurities such as SO<sub>x</sub>, NO<sub>x</sub>, H<sub>2</sub>S, light hydrocarbons, or aromatics, the main concern of feed gases for m-DAC is water [111]. As a condensable gas, it could lead to an increase in free volume, causing a significant decline in performance. In most facilitated transport membranes where amine groups are used as the carriers, the oxidation of carriers by oxidizing gases (mainly O<sub>2</sub>) resulted in the deterioration of membrane performance [111]. The effective pre-treatment of feed gases and exploration of anti-oxidized carriers could help to solve the problem.

Because of the demand for CO<sub>2</sub> at high concentrations, more research needs to focus on multistep and hybrid separation systems [28]. Also, the testing of these systems should be conducted physically with the support of computer modeling. More investigation is

needed on process cost analysis since DAC conditions are different from those operating in typical CO<sub>2</sub> capture, and process cost reductions make the process feasible. Advancements in membrane technology and m-DAC system tunability should be conducted with future downstream applications in mind, which may require a focus on CO<sub>2</sub>/O<sub>2</sub> selectivity and permeate purity [9,12,28]. At the same time, more attention should be brought to using lower purity CO<sub>2</sub> in different utilization pathways with a focus on mixtures of O<sub>2</sub>/N<sub>2</sub>/CO<sub>2</sub> typical of m-DAC [111].

Although most membrane materials do not currently meet the performance criteria for m-DAC, these improved membranes should be further investigated in conjunction with current DAC methods to potentially create more efficient hybrid capture systems. For example, m-DAC can be used as a first separation stage before solid sorbents do the heavy lifting of selective capture. Other innovative ideas, such as membranes used as contactors for liquid solvents or a support structure for solid sorbent monoliths in DAC adsorbers, will inspire researchers to leverage the advantages of the polymeric membrane in DAC processes.

In addition, as suggested by Castro-Muñoz et al., membrane performance should be measured in GPU for permeance rather than Barrer for permeability for standardization across experiments with variability in membrane thickness [26].

Ultimately, the focus of new research should be on increasing membrane permeance, optimizing selectivity, increasing scalability, decreasing cost, and use of hazardous materials, which are commonly associated with DAC methods currently in use. Future m-DAC systems should provide life cycle analyses to finitely determine the extent of negative emissions and operational cost to better illustrate the feasibility of using membranes for direct air capture.

## 7. Conclusions

Increasing CO<sub>2</sub> levels in the atmosphere and 2050 Net Zero Emission requirements have aroused many research efforts in exploring efficient negative CO<sub>2</sub> emission technologies to capture CO<sub>2</sub> from the atmosphere. In the past decades, the intrinsic advantages of membrane technology have promoted its application in CO<sub>2</sub> capture from point sources. Previous efforts in membrane technology have shown the possibility of membrane processes being considered as a new approach to DAC. Due to its great potential for unprecedented improvements in capture cost, installation applications, and environmental impact compared to the current sorbent-based DAC, it is believed that m-DAC will become an important addition to the portfolio of methods aimed at realizing ubiquitous CO<sub>2</sub> capture and could change the outlook on CO<sub>2</sub> capture in the near future. To promote the practical applications of m-DAC, challenges should be overcome through the intersection and application of chemistry, materials science, and engineering. The research on membrane materials is fundamental as the efficiency of m-DAC systems is heavily reliant on the permeance and selectivity of the membranes.

In this mini-review, the required properties of membranes for DAC, process parameters for modeling/system design, potential materials for membranes, and applications of m-DAC have been outlined. Particularly, we summarize the advances up to 2023 in high permeability polymer-based membrane materials for CO<sub>2</sub> separations which could be potential DAC membrane materials, including polymeric membranes, mixed matrix membranes, and CO<sub>2</sub>-facilitated transport membranes. A number of representative examples of recent advances are highlighted, followed by a brief perspective on the direction of future research and development. This work sheds light on the progress of m-DAC and encourages further research at the intersection of disciplines, such as polymer chemistry, inorganic chemistry, nanoscience and technology, and chemical engineering, drawing an inspiring picture of membranes that are more robust, have lower cost and higher CO<sub>2</sub> separation performance.



**Supplementary Materials:** The following supporting information can be downloaded at: <https://www.mdpi.com/article/10.3390/membranes14020030/s1>, Table S1: Summary of recent promising membrane materials showing permeabilities  $\geq 1000$  Barrer or permeances  $> \sim 1000$  GPU or greater with CO<sub>2</sub>/N<sub>2</sub> Selectivity's  $\geq 20$  at temperatures  $\leq 35$  °C; Table S2: CO<sub>2</sub> purity requirements for downstream applications. References [112–176] are cited in the Supplementary Materials.

**Author Contributions:** Writing—original draft preparation, P.I. and N.D.; writing—review and editing, H.L., N.K., L.S., W.M. and B.P. All authors have read and agreed to the published version of the manuscript.

**Funding:** This research was funded by Carbon Capture Utilization and Storage (CCUS) program from Natural Resources Canada's Office of Energy Research and Development (OERD) and Clean Production Program A1-022694 from National Research Council Canada.

**Institutional Review Board Statement:** Not applicable.

**Data Availability Statement:** Data openly available in a public repository that issues datasets with and without DOIs.

**Conflicts of Interest:** The authors declare no conflict of interest.

## References

1. Minx, J.C.; Lamb, W.F.; Callghan, M.W.; Fuss, S.; Hilaire, J.; Creutzig, F.; Amann, T.; Beringer, T.; De Oliveira Garcia, W.; Hartmann, J. Negative emissions-Part1: Research landscape and synthesis. *Environ. Res. Lett.* **2018**, *13*, 063001. [[CrossRef](#)]
2. IPCC. 2023: Summary for Policymakers. In *Climate Change 2023: Synthesis Report. A Report of the Intergovernmental Panel on Climate Change. Contribution of Working Groups I, II and III to the Sixth Assessment Report of the Intergovernmental Panel on Climate Change*; Core Writing Team, Lee, H., Romero, J., Eds.; IPCC: Geneva, Switzerland, 2023; 36p, in press.
3. National Academies of Sciences, Engineering, and Medicine. *Negative Emissions Technologies and Reliable Sequestration: A Research Agenda*; The National Academies Press: Washington, DC, USA, 2019. [[CrossRef](#)]
4. Zhao, C.; Liu, B.; Piao, S.; Wang, X.; Lobell, D.B.; Huang, Y.; Huang, M.; Yao, Y.; Bassu, S.; Ciais, P.; et al. Temperature increase reduces global yields of major crops in four independent estimates. *Proc. Natl. Acad. Sci. USA* **2017**, *114*, 9326–9331. [[CrossRef](#)] [[PubMed](#)]
5. Fujikawa, S.; Selyanchyn, R. Direct air capture by membranes. *MRS Bull.* **2022**, *47*, 416–423. [[CrossRef](#)]
6. Chiwaye, N.; Majozi, T.; Daramola, M.O. On optimisation of N<sub>2</sub> and CO<sub>2</sub>-selective hybrid membrane process systems for post-combustion CO<sub>2</sub> capture from coal-fired power plants. *J. Membr. Sci.* **2021**, *638*, 119691. [[CrossRef](#)]
7. Lackner, K.S.; Brennan, S.; Matter, J.M.; van der Zwaan, B. The urgency of the development of CO<sub>2</sub> capture from ambient air. *Proc. Natl. Acad. Sci. USA* **2012**, *109*, 13156–13162. [[CrossRef](#)] [[PubMed](#)]
8. Shayegh, S.; Bosetti, V.; Tavoni, M. Future Prospects of Direct Air Capture Technologies: Insights from an Expert Elicitation Survey. *Front. Clim.* **2021**, *3*, 630893. [[CrossRef](#)]
9. Ozkan, M. Direct air capture of CO<sub>2</sub>: A response to meet the global climate targets. *MRS. Energy Sustain.* **2021**, *8*, 51–56. [[CrossRef](#)]
10. Beuttler, C.; Charles, L.; Wurzbacher, J. The Role of Direct Air Capture in Mitigation of Anthropogenic Greenhouse Gas Emissions. *Front. Clim.* **2019**, *1*, 10. [[CrossRef](#)]
11. Keith, D.W.; Holmes, G.; St. Angelo, D.; Heidel, K. A Process for Capturing CO<sub>2</sub> from the Atmosphere. *Joule* **2018**, *2*, 1573–1594. [[CrossRef](#)]
12. Fujikawa, S.; Selyanchyn, R.; Kunitake, T. A new strategy for membrane-based direct air capture. *Polym. J.* **2021**, *53*, 111–119. [[CrossRef](#)]
13. Socolow, R.; Desmond, M.; Aines, R.; Blackstock, J.; Bolland, O.; Kaarsberg, T.; Lewis, N.; Mazzotti, M.; Pfeffer, A.; Sawyer, K.; et al. *Direct Air Capture of CO<sub>2</sub> with Chemicals: A Technology Assessment for the APS Panel on Public Affairs*; American Physical Society: College Park, MD, USA, 2011.
14. McQueen, N.; Gomes, K.V.; McCormick, C.; Blumanthal, K.; Pisciotta, M.; Wilcox, J. A review of direct air capture (DAC): Scaling up commercial technologies and innovating for the future. *Prog. Energy* **2021**, *3*, 032001. [[CrossRef](#)]
15. Kikkawa, S.; Anamoto, K.; Fujiki, Y.; Hirayama, J.; Kato, G.; Miura, H.; Shishido, T.; Yamazoe, S. Direct Air Capture of CO<sub>2</sub> Using a Liquid Amine-Solid Carbamic Acid Phase-Separation System Using Diamine Bearing an Aminocyclohexyl Group. *ACS Environ. Au* **2022**, *2*, 354–362. [[CrossRef](#)] [[PubMed](#)]
16. Erans, M.; Sanz-Pérez, E.S.; Hanak, D.P.; Clulow, Z.; Reiner, D.M.; Mutch, G.A. Direct air capture: Process technology, Techno-economic and socio political challenges. *Energy Environ. Sci.* **2022**, *15*, 1360–1405. [[CrossRef](#)]
17. Wiegner, J.F.; Grimm, A.; Weimann, L.; Gazzani, M. Optimal Design and Operation of Solid Sorbent Direct Air Capture Processes at Varying Ambient Conditions. *Ind. Eng. Res.* **2022**, *61*, 12649–12667. [[CrossRef](#)]
18. Lackner, K.S. A Guide to CO<sub>2</sub> Sequestration. *Science* **2003**, *300*, 1677–1678. [[CrossRef](#)] [[PubMed](#)]
19. Osterloh, F.E. The Low Concentration of CO<sub>2</sub> in the Atmosphere Is an Obstacle to a Sustainable Artificial Photosynthesis Fuel Cycle Based on Carbon. *ACS Energy Lett.* **2016**, *1*, 1060–1061. [[CrossRef](#)]

20. Merkel, T.C.; Lin, H.; Wei, X.; Baker, R. Power plant post-combustion carbon dioxide capture: An opportunity for membranes. *J. Membr. Sci.* **2010**, *359*, 126–139. [[CrossRef](#)]
21. Keith, D.W.; Heidel, K.; Cherry, R. *Geoengineering Climate Change. Environment Necessity or Pandora's Box? Capturing CO<sub>2</sub> from Atmosphere: Rationale and Process Design Considerations*; Brian, L., Ed.; Cambridge University Press: Cambridge, UK, 2010; Chapter 6; pp. 107–126.
22. Selyanchyn, R.; Fujikawa, S. Membrane thinning for efficient CO<sub>2</sub> capture. *Sci. Technol. Adv. Mater.* **2017**, *18*, 816–827. [[CrossRef](#)]
23. Xie, K.; Fu, Q.; Qiao, G.G.; Webley, P.A. Recent progress on fabrication of polymeric thin film gas separation membranes for CO<sub>2</sub> capture. *J. Membr. Sci.* **2019**, *572*, 38–60. [[CrossRef](#)]
24. Chen, Y.; Zhao, L.; Wang, B.; Dutta, P.; Ho, W.S.W. Amine-containing polymer/zeolite Y composite membranes for CO<sub>2</sub>/N<sub>2</sub> separation. *J. Membr. Sci.* **2016**, *497*, 21–28. [[CrossRef](#)]
25. Dittmeyer, R.; Klumpp, M.; Kant, P.; Ozin, G. Crowd oil not crude oil. *Nat. Commun.* **2019**, *10*, 1818. [[CrossRef](#)] [[PubMed](#)]
26. Fujikawa, S.; Ariyoshi, M.; Selyanchyn, R.; Kunitake, T. Ultra-fast, Selective CO<sub>2</sub> Permeation by Free-standing Siloxane Nanomembranes. *Chem. Lett.* **2019**, *48*, 1351–1354. [[CrossRef](#)]
27. Setiawan, W.K.; Chiang, K. Amine-functionalized biogenic silica incorporation effect on poly (ether-block-amide) membrane CO<sub>2</sub>/N<sub>2</sub> separation performance. *J. Membr. Sci.* **2023**, *680*, 121732. [[CrossRef](#)]
28. Castro-Muñoz, R.; Ahmad, M.Z.; Malankowska, M.; Coronas, J. A new relevant membrane application: CO<sub>2</sub> direct air capture (DAC). *J. Chem. Eng.* **2022**, *446*, 137047. [[CrossRef](#)]
29. Castel, C.; Bounaceur, R.; Favre, E. Membrane Processes for Direct Carbon Dioxide Capture From Air: Possibilities and Limitations. *Front. Chem. Eng.* **2021**, *3*, 668867. [[CrossRef](#)]
30. Lee, Y.Y.; Gurkan, B. Graphene oxide reinforced facilitated transport membrane with poly(ionic liquid) and ionic liquid carriers for CO<sub>2</sub>/N<sub>2</sub> separation. *J. Membr. Sci.* **2021**, *638*, 119652. [[CrossRef](#)]
31. Yave, W.; Car, A.; Wind, J.; Peinemann, K. Nanometric thin film membranes manufactured on square meter scale: Ultra-thin films for CO<sub>2</sub> capture. *Nanotechnology* **2010**, *21*, 395301. [[CrossRef](#)]
32. Selyanchyn, C.; Selyanchyn, R.; Fujikawa, S. Critical Role of the Molecular Interface in Double-Layered Pebax-1657/PDMS Nanomembranes for Highly Efficient CO<sub>2</sub>/N<sub>2</sub> Gas Separation. *ACS Appl. Mater. Interfaces* **2020**, *12*, 33196–33209. [[CrossRef](#)]
33. Yoo, M.J.; Kim, K.H.; Lee, J.H.; Kim, T.W.; Chung, C.W.; Cho, Y.H.; Park, H.B. Ultrathin gutter layer for high-performance thin-film composite membranes for CO<sub>2</sub> separation. *J. Membr. Sci.* **2018**, *566*, 336–345. [[CrossRef](#)]
34. Seppänen, O.A.; Fisk, W.J.; Mendell, W.J. Association of Ventilation Rates and CO<sub>2</sub> Concentrations with Health and Other Responses in Commercial and Institutional Buildings. *Indoor Air* **1999**, *9*, 226–252. [[CrossRef](#)]
35. Mohsenpour, S.; Guo, Z.; Almansour, F.; Holmes, S.M.; Budd, P.M.; Gorgojo, P. Porous silica nanosheets in PIM-1 membranes for CO<sub>2</sub> separation. *J. Membr. Sci.* **2022**, *661*, 120889. [[CrossRef](#)]
36. Vendamme, R.; Onoue, S.; Nakao, A.; Kunitake, T. Robust free-standing membranes of organic/inorganic interpenetrating networks. *Nat. Mater.* **2006**, *5*, 494–501. [[CrossRef](#)] [[PubMed](#)]
37. Wanatabe, H.; Kunitake, T. A Large, Freestanding, 20 nm Thick Nanomembrane Based on an Epoxy Resin. *Adv. Mater.* **2007**, *19*, 909–912. [[CrossRef](#)]
38. He, S.; Zhu, B.; Li, S.; Zhang, Y.; Jiang, X.; Lau, C.H.; Shao, L. Recent progress in PIM-1 based membranes for sustainable CO<sub>2</sub> separations: Polymer structure manipulation and mixed matrix membrane design. *Sep. Purif. Technol.* **2022**, *284*, 120277. [[CrossRef](#)]
39. Robeson, L.M. The upper bound revisited. *J. Membr. Sci.* **2008**, *320*, 390–400. [[CrossRef](#)]
40. Swaidan, R.; Al-Saeedi, M.; Ghanem, B.; Litwiller, E.; Pinnau, I. Rational Design of Intrinsically Ultramicroporous Polyimides Containing Bridgehead-Substituted Triptycene for Highly Selective and Permeable Gas Separation Membranes. *Macromolecules* **2014**, *47*, 5104–5114. [[CrossRef](#)]
41. Comesaña-Gándara, B.; Chen, J.; Bezzu, B.G.; Carta, M.; Rose, I.; Ferrari, M.; Esposito, E.; Fuoco, A.; Jansen, J.C.; Mckeown, N.B. Redefining the Robeson upper bounds for CO<sub>2</sub>/CH<sub>4</sub> and CO<sub>2</sub>/N<sub>2</sub> separations using a series of ultrapermeable benzotriptycene-based polymers of intrinsic microporosity. *Energy Environ. Sci.* **2019**, *12*, 2733–2740. [[CrossRef](#)]
42. Shrimant, B.; Kharul, U.K.; Wadgaonkar, P.P. Spiro[fluorene-9,9'-xanthene]-containing copolymers of intrinsic microporosity: Synthesis, characterization and gas permeation properties. *React. Funct. Polym.* **2018**, *133*, 153–160. [[CrossRef](#)]
43. Sun, W.; Yin, M.; Zhang, W.; Li, S.; Wang, N.; An, Q. Green Techniques for Rapid Fabrication of Unprecedentedly High-Performance PEO Membranes for CO<sub>2</sub> Capture. *ACS Sustain. Chem. Eng.* **2021**, *9*, 10167–10175. [[CrossRef](#)]
44. Nazarov, I.V.; Khrychikova, A.P.; Medentseva, E.I.; Bermesheva, E.V.; Borisov, I.L.; Yushkin, A.A.; Volkov, A.V.; Wozniak, A.I.; Petukhov, D.I.; Topchiy, M.A.; et al. CO<sub>2</sub>-selective vinyl-addition polymers from nadimides: Synthesis and performance for membrane gas separation. *J. Membr. Sci.* **2023**, *677*, 121624. [[CrossRef](#)]
45. Alentiev, D.A.; Egorova, E.S.; Bermeshev, M.V.; Starannikova, L.E.; Topchiy, M.A.; Asachenko, A.F.; Griбанov, P.S.; Nechaev, M.S.; Yampolskii, Y.P.; Finkelshtein, E.S. Janus tricyclononene polymers bearing tri(n-alkoxy)silyl side groups for membrane gas separation. *J. Mater. Chem. A* **2018**, *6*, 19393–19408. [[CrossRef](#)]
46. White, L.S.; Amo, K.D.; Wu, T.; Markel, T.C. Extended field trials of Polaris sweep modules for carbon capture. *J. Membr. Sci.* **2017**, *542*, 217–225. [[CrossRef](#)]
47. Brinkmann, T.; Lillepär, J.; Notzke, H.; Pohlmann, J.; Shishatskiy, S.; Wind, J.; Wolff, T. Development of CO<sub>2</sub> selective poly(ethylene oxide)-based membranes: From laboratory to pilot plant scale. *Engineering* **2017**, *3*, 485–493. [[CrossRef](#)]

48. Du, N.; Park, H.B.; Robertson, G.P.; Dal-Cin, M.M.; Visser, T.; Scoles, L.; Guiver, M.D. Polymer nanosieve membranes for CO<sub>2</sub>-capture applications. *Nat. Mater.* **2011**, *10*, 372–375. [[CrossRef](#)] [[PubMed](#)]
49. Swaidan, R.; Ghanem, B.S.; Litwiller, E.; Pinnau, I. Pure- and mixed-gas CO<sub>2</sub>/CH<sub>4</sub> separation properties of PIM-1 and an amidoxime-functionalized PIM-1. *J. Membr. Sci.* **2014**, *457*, 95–102. [[CrossRef](#)]
50. Du, N.; Robertson, G.P.; Dal-Cin, M.M.; Scoles, L.; Guiver, M.D. Polymers of intrinsic microporosity (PIMs) substituted with methyl tetrazole. *Polymer* **2012**, *53*, 4367–4372. [[CrossRef](#)]
51. Manson, C.R.; Maynard-Atem, L.; Al-Harbi, N.M.; Budd, P.M.; Bernardo, P.; Bazzarelli, F.; Clarizia, G.; Jansen, J.C. Polymer of intrinsic Microporosity Incorporating Thioamide Functionality: Preparation and Gas Transport Properties. *Macromolecules* **2011**, *44*, 6471–6479. [[CrossRef](#)]
52. Han, W.; Zhang, C.; Zhao, M.; Yang, F.; Yang, Y.; Weng, Y. Post-modification of PIM-1 and simultaneously in situ synthesis of porous polymer networks into PIM-1 matrix to enhance CO<sub>2</sub> separation performance. *J. Membr. Sci.* **2021**, *636*, 119544. [[CrossRef](#)]
53. Nafisi, V.; Hägg, M. Development of Nanocomposite Membranes Containing Modified Si Nanoparticles in PEBAX-2533 as a Block Co-polymer and 6FDA-Durene Diamine as a Glassy Polymer. *ACS Appl. Mater. Interfaces* **2014**, *6*, 15643–15652. [[CrossRef](#)]
54. Mason, C.R.; Buonomenna, M.G.; Golemme, G.; Budd, P.M.; Galiano, F.; Figoli, A.; Friess, K.; Hynek, V. New organophilic mixed matrix membranes derived from a polymer of intrinsic microporosity and silicalite-1. *Polymer* **2013**, *54*, 2222–2230. [[CrossRef](#)]
55. Nafisi, V.; Hägg, M. Development of dual layer of ZIF-8/PEBAX-2533 mixed matrix membrane for CO<sub>2</sub> capture. *J. Membr. Sci.* **2014**, *459*, 244–255. [[CrossRef](#)]
56. Xin, Q.; Liu, T.; Li, Z.; Wang, S.; Li, Y.; Li, Z.; Ouyang, J.; Jiang, Z.; Wu, H. Mixed matrix membranes composed of sulfonated poly(ether ether ketone) and a sulfonated metal–organic framework for gas separation. *J. Membr. Sci.* **2015**, *488*, 67–78. [[CrossRef](#)]
57. Yu, G.; Zou, X.; Sun, L.; Liu, B.; Wang, Z.; Zhang, P.; Zhu, G. Constructing Connected Paths between UiO-66 and PIM-1 to improve Membrane CO<sub>2</sub> Separation with Crystal-Like Gas Selectivity. *Adv. Mater.* **2019**, *31*, e1806853. [[CrossRef](#)] [[PubMed](#)]
58. Haider, B.; Dilshad, M.R.; Akram, M.S.; Islam, A.; Kaspereit, M. Novel Polydimethylsiloxane membranes impregnated with SAPO-34 zeolite particles for gas separation. *Chem. Pap.* **2021**, *75*, 6417–6431. [[CrossRef](#)]
59. Chen, M.; Soyekwo, F.; Zhang, Q.; Hu, C.; Zhu, A.; Liu, Q. Graphene oxide nanosheets to improve permeability and selectivity of PIM-1 membrane for carbon dioxide separation. *J. Ind. Eng. Chem.* **2018**, *63*, 296–302. [[CrossRef](#)]
60. Ashtiani, S.; Sofer, Z.; Průša, F.; Friess, K. Molecular-level fabrication of highly selective composite ZIF-8-CNT-PDMS membranes for effective CO<sub>2</sub>/N<sub>2</sub>, CO<sub>2</sub>/H<sub>2</sub> and olefin/paraffin separations. *Sep. Purif. Technol.* **2021**, *274*, 119003. [[CrossRef](#)]
61. Wang, Z.; Ren, H.; Zhang, S.; Zhang, F.; Jin, J. Polymers of intrinsic microporosity/metal-organic framework hybrid membranes with improved interfacial interaction for high-performance CO<sub>2</sub> separation. *J. Mater. Chem. A* **2017**, *5*, 10968–10977. [[CrossRef](#)]
62. Ding, X.; Tan, F.; Zhao, H.; Hua, M.; Wang, M.; Xin, Q.; Zhang, Y. Enhancing gas permeation and separation performance of polymeric membrane by incorporating hollow polyamide nanoparticles with dense shell. *J. Membr. Sci.* **2019**, *570–571*, 53–60. [[CrossRef](#)]
63. Li, X.; Ding, S.; Zhang, J.; Wei, Z. Optimizing microstructure of polymer composite membranes by tailoring different ionic liquids to accelerate CO<sub>2</sub> transport. *Int. J. Greenh. Gas Control* **2020**, *101*, 103136. [[CrossRef](#)]
64. Liu, Y.; Yu, S.; Wu, H.; Li, Y.; Wang, S.; Tian, Z.; Jiang, Z. High permeability hydrogel membranes of chitosan/poly ether-block-amide blends for CO<sub>2</sub> separation. *J. Membr. Sci.* **2014**, *469*, 198–208. [[CrossRef](#)]
65. Wu, H.; Li, X.; Li, Y.; Wang, S.; Guo, R.; Jiang, Z.; Wu, C.; Xin, Q.; Lu, X. Facilitated transport mixed matrix membranes incorporated with amine functionalized MCM-41 for enhanced gas separation properties. *J. Membr. Sci.* **2014**, *465*, 78–90. [[CrossRef](#)]
66. Mashhadikhan, S.; Moghadassi, A.; Amooghin, A.E.; Sanaeepur, H. Interlocking a synthesized polymer and bifunctional filler containing the same polymer's monomer for conformable hybrid membrane systems. *J. Mater. Chem. A* **2020**, *8*, 3942–3955. [[CrossRef](#)]
67. Zhao, D.; Ren, J.; Wang, Y.; Qiu, Y.; Li, H.; Hua, K.; Li, X.; Ji, J.; Deng, M. High CO<sub>2</sub> separation performance of Pebax<sup>®</sup>/CNTs/GTA mixed matrix membranes. *J. Membr. Sci.* **2017**, *521*, 104–113. [[CrossRef](#)]
68. Zhang, H.; Tian, H.; Zhang, J.; Guo, R.; Li, X. Facilitated transport membranes with an amino acid salt for highly efficient CO<sub>2</sub> separation. *Int. J. Greenh. Gas Control* **2018**, *78*, 85–93. [[CrossRef](#)]
69. Akbarzadeh, E.; Shockravi, A.; Vatanpour, V. High performance compatible thiazole-based polymeric blend cellulose acetate membrane as selective CO<sub>2</sub> absorbent and molecular sieve. *Carbohydr. Polym.* **2021**, *252*, 117215. [[CrossRef](#)] [[PubMed](#)]
70. Wang, C.; Guo, F.; Li, H.; Xu, J.; Hu, J.; Liu, H.; Wang, M. A porous ionic polymer bionic carrier in a mixed matrix membrane for facilitating selective CO<sub>2</sub> permeability. *J. Membr. Sci.* **2020**, *598*, 117215. [[CrossRef](#)]
71. Yu, M.; Foster, A.B.; Alshurafa, M.; Luque-Alled, J.M.; Gorgojo, P.; Kentish, S.E.; Scholes, C.A.; Budd, P.M. CO<sub>2</sub> separation using thin film composite membranes of acid-hydrolyzed PIM-1. *J. Membr. Sci.* **2023**, *679*, 121697. [[CrossRef](#)]
72. Swaidan, R.; Ghanem, B.; Litwiller, E.; Pinnau, I. Physical Aging, Plasticization and Their Effects on Gas Permeation in “Rigid” Polymers of Intrinsic Microporosity. *Macromolecules* **2015**, *48*, 6553–6561. [[CrossRef](#)]
73. Ahmad, M.Z.; Castro-Muñoz, R.; Budd, P.M. Boosting gas separation performance and suppressing the physical aging of polymers of intrinsic microporosity (PIM-1) by nanomaterial blending. *Nanoscale* **2020**, *12*, 23333–23370. [[CrossRef](#)]
74. Norahim, N.; Yaisanga, P.; Faungnawakij, K.; Charinpanitkul, T.; Klayson, C. Recent Membrane Developments for CO<sub>2</sub> Separation and Capture. *Chem. Eng. Technol.* **2018**, *41*, 211–223. [[CrossRef](#)]



75. Budd, P.M.; Msayib, K.J.; Tattershall, C.E.; Ghanem, B.S.; Reynolds, K.J.; McKeown, N.B.; Fritsch, D. Gas separation membranes from polymers of intrinsic microporosity. *J. Membr. Sci.* **2005**, *251*, 263–269. [[CrossRef](#)]
76. Wang, Y.; Ma, X.; Ghanem, B.S.; Alghunaimi, F.; Pinnau, I.; Han, Y. Polymers of intrinsic microporosity for energy-intensive membrane-based gas separations. *Mater. Today Nano* **2018**, *3*, 69–95. [[CrossRef](#)]
77. Han, X.; Zhang, J.; Yue, C.; Pang, J.; Zhang, H.; Jiang, Z. Novel copolymers with intrinsic microporosity containing tetraphenylbipyrimidine for enhanced gas separation. *J. Ind. Eng. Chem.* **2020**, *91*, 102–109. [[CrossRef](#)]
78. Bezzu, C.G.; Carta, M.; Ferrari, M.; Jansen, J.C.; Monteleone, M.; Elisa, E.; Fuoco, A.; Hart, K.; Liyana-Arachchi, T.P.; Colina, C.M.; et al. The synthesis, chain-packing simulation and long-term gas permeability of highly selective spirobifluorene-based polymers of intrinsic microporosity. *J. Mater. Chem A* **2018**, *6*, 10507–10514. [[CrossRef](#)]
79. Zhu, B.; Jiang, X.; He, S.; Xiaobin, Y.; Long, J.; Zhang, Y.; Shao, L. Rational design of poly(ethylene oxide) based membranes for sustainable CO<sub>2</sub> capture. *J. Mater. Chem. A* **2020**, *8*, 24233–24252. [[CrossRef](#)]
80. Bandehali, S.; Moghadassi, A.; Parvizian, F.; Hosseini, S.M.; Matsuura, T.; Joudaki, E. Advances in high carbon dioxide separation performance of poly (ethylene oxide)-based membranes. *J. Energy Chem.* **2020**, *46*, 30–52. [[CrossRef](#)]
81. Han, Y.; Ho, W.S.W. Recent advances in polymeric membranes for CO<sub>2</sub> capture. *Chin. J. Chem. Eng.* **2018**, *26*, 2238–2254. [[CrossRef](#)]
82. Rogan, Y.; Starannikova, L.; Ryzhikh, V.; Yampolskii, V.; Yampolskii, Y.; Bernardo, P.; Bazzarelli, F.; Jansen, J.C.; McKeown, N.B. Synthesis and gas permeation properties of novel spirobisindane-based polyimides of intrinsic microporosity. *Polym. Chem.* **2013**, *4*, 1820–3813. [[CrossRef](#)]
83. Ghanem, B.S.; McKeown, N.B.; Budd, P.M.; Al-Harbi, N.M.; Fritsch, D.; Heinrich, K.; Starannikova, L.; Tokarev, A.; Yampolskii, Y. Synthesis, Characterization, and Gas Permeation Properties of a Novel Group of Polymers with Intrinsic Microporosity: PIM-Polyimides. *Macromolecules* **2009**, *42*, 7881–7888. [[CrossRef](#)]
84. Song, Q.; Cao, S.; Zavala-Rivera, P.; Lu, L.P.; Li, W.; Ji, Y.; Al-Muhtaseb, S.A.; Cheetham, A.K.; Sivaniah, E. Photo-oxidative enhancement of polymeric molecular sieve membranes. *Nat. Commun.* **2013**, *4*, 1918. [[CrossRef](#)]
85. Song, Q.; Cao, S.; Pritchard, R.H.; Ghalei, B.; Al-Muhtaseb, S.A.; Terentjev, E.M.; Cheetham, A.K.; Sivaniah, E. Controlled thermal oxidative crosslinking of polymers of intrinsic microporosity towards tunable molecular sieve membranes. *Nat. Commun.* **2014**, *5*, 4813. [[CrossRef](#)] [[PubMed](#)]
86. Li, F.Y.; Xiao, Y.; Chung, T.; Kawi, S. High-Performance Thermally Self-Cross-Linked Polymer of Intrinsic Microporosity (PIM-1) Membranes for Energy Development. *Macromolecules* **2012**, *45*, 1427–1437. [[CrossRef](#)]
87. Luo, S.; Zhang, Q.; Zhu, L.; Lin, H.; Kazanowska, B.A.; Doherty, C.M.; Hill, A.J.; Gao, P.; Guo, R. Highly Selective and Permeable Microporous Polymer Membranes for Hydrogen Purification and CO<sub>2</sub> Removal from Natural Gas. *Chem. Matter.* **2018**, *30*, 5322–5332. [[CrossRef](#)]
88. Ma, X.; Salinas, O.; Litwiller, E.; Pinnau, I. Pristine and thermally-rearranged gas separation membranes for novel o-hydroxyl-functionalized spirobifluorene-based polyimides. *Polym. Chem.* **2014**, *5*, 6913–6922. [[CrossRef](#)]
89. Bandehali, S.; Amooghin, A.E.; Sanaeepur, H.; Ahmadi, R.; Fuoco, A.; Jansen, J.C.; Shirazian, S. Polymers of intrinsic microporosity and thermally rearranged polymer membranes for highly efficient gas separation. *Sep. Purif. Technol.* **2021**, *278*, 119513. [[CrossRef](#)]
90. Janakiram, S.; Ahmadi, M.; Dai, Z.; Ansaloni, L.; Deng, L. Performance of Nanocomposite Membranes Containing 0D to 2D Nanofillers for CO<sub>2</sub> Separation: A Review. *Membranes* **2018**, *8*, 24. [[CrossRef](#)]
91. Liu, M.; Nothling, M.D.; Webly, P.A.; Jin, J.; Fu, Q.; Qiao, G.G. High-throughput CO<sub>2</sub> capture using PIM-1@MOF based thin film composite membranes. *J. Chem. Eng.* **2020**, *396*, 125328. [[CrossRef](#)]
92. Muldoon, P.F.; Venna, S.R.; Gidley, D.W.; Baker, J.S.; Zhu, L.; Tong, Z.; Xiang, F.; Hopkinson, D.P.; Yi, S.; Sekizkardes, A.K.; et al. Mixed Matrix Membranes from a Microporous Polymer Blend and Nanosized Metal-Organic Frameworks with Exceptional CO<sub>2</sub>/N<sub>2</sub> Separation Performance. *ACS Mater. Lett.* **2020**, *2*, 821–828. [[CrossRef](#)]
93. Fan, S.; Wang, J.; Liao, L.; Feng, J.; Li, B.; Zhang, S. Enhanced selectivity in thin film composite membrane for CO<sub>2</sub> capture through improvement to support layer. *J. Chem. Eng.* **2023**, *468*, 143645. [[CrossRef](#)]
94. Lin, Z.; Yuan, Z.; Wang, K.; He, X. Synergistic tuning mixed matrix membranes by Ag<sup>+</sup>-doping in UiO-66-NH<sub>2</sub>/polymers of intrinsic microporosity for remarkable CO<sub>2</sub>/N<sub>2</sub> separation. *J. Membr. Sci.* **2023**, *681*, 121775. [[CrossRef](#)]
95. Messaoud, S.B.; Takagaki, A.; Sugawara, T.; Kikuchi, R.; Oyama, S.T. Mixed matrix membranes using SAPO-34/polyetherimide for carbon dioxide/methane separation. *Sep. Purif. Technol.* **2015**, *148*, 38–48. [[CrossRef](#)]
96. Li, X.; Ma, L.; Zhang, H.; Wang, S.; Jiang, Z.; Guo, R.; Wu, H.; Cao, X.; Yang, J.; Wang, B. Synergistic effect of combining carbon nanotubes and graphene oxide in mixed matrix membranes for efficient CO<sub>2</sub> separation. *J. Membr. Sci.* **2015**, *479*, 1–10. [[CrossRef](#)]
97. Wang, S.; Li, X.; Wu, H.; Tian, Z.; Xin, Q.; He, G.; Peng, D.; Chen, S.; Yin, Y.; Jiang, Z.; et al. Advances in high permeability polymer-based membrane materials for CO<sub>2</sub> separations. *Energy Environ. Sci.* **2016**, *9*, 1863–1890. [[CrossRef](#)]
98. Seong, M.K.; Yu, H.J.; Ha, S.Y.; Chang, W.S.; Kim, H.; Lee, J.S. Poly(poly(ethylene glycol) methyl ether acrylate) micelles for highly CO<sub>2</sub> permeable membranes. *J. Membr. Sci.* **2022**, *662*, 120917. [[CrossRef](#)]
99. Jiang, X.; Li, S.; Shao, L. Pushing CO<sub>2</sub>-philic membrane performance to the limit by designing semi-interpenetrating networks (SIPN) for sustainable CO<sub>2</sub> separations. *Energy Environ. Sci.* **2017**, *10*, 1339–1344. [[CrossRef](#)]
100. Chen, S.; Zhao, D.; Feng, Y.; Liu, H.; Li, S.; Qiu, Y.; Ren, J. The preparation and characterization of gel-mixed matrix membranes (g-MMMs) with high CO<sub>2</sub> permeability and stability performance. *J. Membr. Sci.* **2022**, *652*, 120471. [[CrossRef](#)]

101. Guo, H.; Wei, J.; Deng, J.; Yi, S.; Wang, B.; Deng, L.; Jiang, X.; Dai, Z. Facilitated transport membranes for CO<sub>2</sub>/CH<sub>4</sub> separation—State of the art. *Adv. Membr.* **2022**, *2*, 100040. [[CrossRef](#)]
102. Hong, C.; Leo, C.P.; Ahmad, N.N.R.; Ahmad, A.L.; Mohammad, A.W. Polyvinyl alcohol membrane incorporated with amine-modified silica nanoparticles and ionic liquid for facilitated transport of CO<sub>2</sub>. *Int. J. Greenh. Gas Control* **2022**, *120*, 103774. [[CrossRef](#)]
103. Costa, S.P.F.; Azevedo, A.M.O.; Pinto, P.C.A.G.; Saraiva, M.L.M.F.S. Environmental Impact of Ionic Liquids: Recent Advances in (Eco)toxicology and (Bio)degradability. *Eur. J. Chem.* **2017**, *10*, 2321–2347. [[CrossRef](#)]
104. Han, Y.; Ho, W.S.W. Recent advances in polymeric facilitated transport membranes for carbon dioxide separation and hydrogen purification. *J. Polym. Sci.* **2020**, *58*, 2435–2449. [[CrossRef](#)]
105. IEAGHG. *Effects of Impurities on Geological Storage of CO<sub>2</sub>*; IEAGHG: Cheltenham, UK, 2011.
106. Anantharaman, R.; Berstad, D.; Roussanaly, S. Techno-economic Performance of a Hybrid Membrane—Liquefaction Process for Post-combustion CO<sub>2</sub> Capture. *Energy Procedia* **2014**, *61*, 1244–1247. [[CrossRef](#)]
107. Sreenath, S.; Sam, A.A. Hybrid membrane-cryogenic CO<sub>2</sub> capture technologies: A mini-review. *Front. Energy Res.* **2023**, *11*, 1167024. [[CrossRef](#)]
108. Belaissaoul, B.; Le Moullec, Y.; Willson, D.; Favre, E. Hybrid membrane cryogenic process for post-combustion CO<sub>2</sub> capture. *J. Membr. Sci.* **2012**, *415–416*, 424–434. [[CrossRef](#)]
109. Zhang, Z.; Pan, S.; Li, H.; Cai, J.; Olabi, A.G.; Anthony, E.J.; Manovic, V. Recent advances in carbon dioxide utilization. *Renew. Sustain. Energy Rev.* **2020**, *25*, 109799. [[CrossRef](#)]
110. Kim, B.; Ma, S.; Jhong, H.M.; Kenis, P.J. Influence of dilute feed and pH on electrochemical reduction of CO<sub>2</sub> to CO on Ag in a continuous flow electrolyzer. *Electrochim. Acta* **2015**, *166*, 271–276. [[CrossRef](#)]
111. Tsuji, T.; Sorai, M.; Shiga, M.; Fujikawa, S.; Kunitake, T. Geological storage of CO<sub>2</sub>-N<sub>2</sub>-O<sub>2</sub> mixtures produced by membrane-based direct air capture (DAC). *Greenh. Gases Sci. Technol.* **2021**, *11*, 610–618. [[CrossRef](#)]
112. Longo, M.; De Santo, M.P.; Esposito, E.; Fuoco, A.; Monteleone, M.; Giorno, L.; Comesaña-Gándara, B.; Chen, J.; Bezzu, C.G.; Carta, M.; et al. Correlating Gas Permeability and Young's Modulus during the Physical Aging of Polymers of Intrinsic Microporosity Using Atomic Force Microscopy. *Ind. Eng. Chem. Res.* **2020**, *12*, 5381–5391. [[CrossRef](#)]
113. Carta, M.; Bernardo, P.; Clarizia, G.; Jansen, J.C.; McKeown, N.B. Gas Permeability of Hexaphenylbenzene Based Polymers of Intrinsic Microporosity. *Macromol.* **2014**, *47*, 8320–8327. [[CrossRef](#)]
114. Santiago-García, J.L.; Álvarez, C.; Sánchez, F.; de la Campa, J.G. Gas transport properties of new aromatic polyimides based on 3,8-diphenylpyrene-1,2,6,7-tetracarboxylic dianhydride. *J. Membr. Sci.* **2015**, *476*, 442–448. [[CrossRef](#)]
115. Ma, X.; Pinnau, I. A novel intrinsically microporous ladder polymer and copolymers derived from 1,1',2,2'-tetrahydroxytetraphenylethylene for membrane-based gas separation. *Polym. Chem.* **2016**, *7*, 1244–1248. [[CrossRef](#)]
116. Wang, Z.; Wang, D.; Jin, J. Microporous Polyimides with Rationally Designed Chain Structure Achieving High Performance for Gas Separation. *Macromol.* **2014**, *47*, 7477–7483. [[CrossRef](#)]
117. Ma, X.; Zhu, Z.; Shi, W.; Ji, W.; Li, J.; Wang, Y.; Pinnau, I. Unprecedented gas separation performance of difluoro-functionalized triptycene-based ladder PIM membrane at low temperature. *J. Mater. Chem. A* **2021**, *9*, 5404–5414. [[CrossRef](#)]
118. Ghanem, B.S.; Swaidan, R.; Ma, X.; Litwiller, E.; Pinnau, I. Energy-Efficient Hydrogen Separation by AB-Type Ladder-Polymer Molecular Sieves. *Adv. Mater.* **2014**, *26*, 6696–6700. [[CrossRef](#)] [[PubMed](#)]
119. Ghanem, B.S.; Alghunaimi, F.; Wang, Y.; Genduso, G.; Pinnau, I. Synthesis of Highly Gas-Permeable Polyimides of Intrinsic Microporosity Derived from 1,3,6,8-Tetramethyl-2,7-diaminotriptycene. *ACS Omega* **2018**, *3*, 11874–11882. [[CrossRef](#)] [[PubMed](#)]
120. Hu, X.; Lee, W.H.; Bae, J.Y.; Zhao, J.; Kim, J.S.; Wang, Z.; Yan, J.; Lee, Y.M. Highly permeable polyimides incorporating Tröger's base (TB) units for gas separation membranes. *J. Membr. Sci.* **2020**, *615*, 118533. [[CrossRef](#)]
121. Ma, X.; Ghanem, B.; Salines, O.; Litwiller, E.; Pinnau, I. Synthesis and Effect of Physical Aging on Gas Transport Properties of a Microporous Polyimide Derived from a Novel Spirobifluorene-Based Dianhydride. *ACS Macro Lett.* **2015**, *4*, 231–235. [[CrossRef](#)] [[PubMed](#)]
122. Ma, X.; Abdulhamid, M.A.; Pinnau, I. Design and Synthesis of Polyimides Based on Carbocyclic Pseudo-Tröger's Base-Derived Dianhydrides for Membrane Gas Separation Applications. *Macromolecules* **2017**, *50*, 5850–5857. [[CrossRef](#)]
123. Esposito, E.; Mazzei, I.; Monteleone, M.; Fuoco, A.; Carta, M.; McKeown, N.B.; Mapass-Evans, R.; Jansen, J.C. Highly Permeable Matrimid®/PIM-EA(H2)-TB Blend Membrane for Gas Separation. *Polymers* **2019**, *11*, 46. [[CrossRef](#)]
124. Carta, M.; Croad, M.; Malpass-Evans, R.; Jansen, J.C.; Bernardo, P.; Clarizia, G.; Friess, K.; Lanč, M.; McKeown, N.B. Triptycene Induced Enhancement of Membrane Gas Selectivity for Microporous Tröger's Base Polymers. *Adv. Mater.* **2014**, *26*, 3526–3531. [[CrossRef](#)]
125. Fritsch, D.; Bengtson, G.; Carta, M.; McKeown, N.B. Synthesis and Gas Permeation Properties of Spirobischromane-based Polymers of Intrinsic Microporosity. *Macromol. Chem. Phys.* **2011**, *212*, 1137–1146. [[CrossRef](#)]
126. Yuan, K.; Liu, C.; Zhang, S.; Jiang, L.; Liu, C.; Yu, G.; Wang, J.; Jian, X. Phthalazinone-based copolymers with intrinsic microporosity (PHPIMs) and their separation performance. *J. Membr. Sci.* **2017**, *541*, 403–412. [[CrossRef](#)]
127. Jiang, X.; Goh, K.; Wang, R. Air plasma assisted spray coating of Pebax-1657 thin-film composite membranes for post-combustion CO<sub>2</sub> capture. *J. Membr. Sci.* **2022**, *658*, 120741. [[CrossRef](#)]
128. Zhang, G.; Tran, N.T.; Huang, L.; Deng, E.; Blevins, A.; Guo, W.; Ding, Y.; Lin, H. Thin-film composite membranes based on hyperbranched poly(ethylene oxide) for CO<sub>2</sub>/N<sub>2</sub> separation. *J. Membr. Sci.* **2022**, *644*, 120184. [[CrossRef](#)]



129. Li, S.; Wang, Z.; Zhang, C.; Wang, M.; Yuan, F.; Wang, J.; Wang, S. Interfacially polymerized thin film composite membranes containing ethylene oxide groups for CO<sub>2</sub> separation. *J. Membr. Sci.* **2013**, *436*, 121–131. [[CrossRef](#)]
130. Chua, M.L.; Xiao, Y.C.; Chung, T. Effects of thermally labile saccharide units on the gas separation performance of highly permeable polyimide membranes. *J. Membr. Sci.* **2012**, *415–416*, 375–382. [[CrossRef](#)]
131. Do, Y.S.; Lee, W.H.; Seong, J.G.; Kim, J.S.; Wang, H.H.; Doherty, C.M.; Hill, A.J.; Lee, Y.M. Thermally rearranged (TR) bismaleimide-based network polymers for gas separation membranes. *Chem. Commun.* **2016**, *52*, 13556–13559. [[CrossRef](#)] [[PubMed](#)]
132. Kim, S.; Jo, H.J.; Lee, Y.M. Sorption and transport of small gas molecules in thermally rearranged (TR) polybenzoxazole membranes based on 2,2-bis(3-amino-4-hydroxyphenyl)-hexafluoropropane (bisAPAF) and 4,4'-hexafluoroisopropylidene diphthalic anhydride (6FDA). *J. Membr. Sci.* **2013**, *441*, 1–8. [[CrossRef](#)]
133. Han, S.H.; Lee, J.E.; Lee, K.; Park, H.B.; Lee, Y.M. Highly gas permeable and microporous polybenzimidazole membrane by thermal rearrangement. *J. Membr. Sci.* **2010**, *357*, 143–151. [[CrossRef](#)]
134. Choi, J.I.; Jung, C.H.; Han, S.H.; Park, H.B.; Lee, Y.M. Thermally rearranged (TR) poly(benzoxazole-co-pyrrolone) membranes tuned for high gas permeability and selectivity. *J. Membr. Sci.* **2010**, *349*, 358–368. [[CrossRef](#)]
135. Du, N.; Dal-Cin, M.M.; Robertson, G.P.; Guiver, M.D. Decarboxylation-Induced Cross-Linking of Polymers of Intrinsic Microporosity (PIMs) for Membrane Gas Separation. *Macromolecules* **2012**, *45*, 5134–5139. [[CrossRef](#)]
136. Li, F.Y.; Xiao, Y.; Ong, Y.K.; Chung, T. UV-Rearranged PIM-1 Polymeric Membranes for Advanced Hydrogen Purification and Production. *Adv. Energy Mater.* **2012**, *2*, 1456–1466. [[CrossRef](#)]
137. Sun, Y.; Zhang, J.; Li, H.; Fan, F.; Zhao, Q.; He, G.; Ma, C. Ester-crosslinked polymers of intrinsic microporosity membranes with enhanced plasticization resistance for CO<sub>2</sub> separation. *Sep. Purif. Technol.* **2023**, *314*, 123623. [[CrossRef](#)]
138. Hazazi, K.; Ma, X.; Wang, Y.; Ogieglo, W.; Alhazmi, A.; Han, Y.; Pinnau, I. Ultra-selective carbon molecular sieve membranes for natural gas separations based on a carbon-rich intrinsically microporous polyimide precursor. *J. Membr. Sci.* **2019**, *585*, 1–9. [[CrossRef](#)]
139. Chuah, C.Y.; Lee, J.; Bao, Y.; Song, J.; Bae, T. High-performance porous carbon-zeolite mixed-matrix membranes for CO<sub>2</sub>/N<sub>2</sub> separation. *J. Membr. Sci.* **2021**, *622*, 119031. [[CrossRef](#)]
140. Chi, W.S.; Kim, S.J.; Lee, S.; Bae, Y.; Kim, J.H. Enhanced Performance of Mixed-Matrix Membranes through a Graft Copolymer-Directed Interface and Interaction Tuning Approach. *ChemSusChem* **2014**, *8*, 650–658. [[CrossRef](#)] [[PubMed](#)]
141. Min, H.J.; Kang, M.; Bae, Y.; Blom, R.; Grande, C.A.; Kim, J.H. Thin-film composite mixed-matrix membrane with irregular micron-sized UTSA-16 for outstanding gas separation performance. *J. Membr. Sci.* **2023**, *669*, 121295. [[CrossRef](#)]
142. Luo, W.; Niu, Z.; Mu, P.; Li, J. MXene/poly(ethylene glycol) mixed matrix membranes with excellent permeance for highly efficient separation of CO<sub>2</sub>/N<sub>2</sub> and CO<sub>2</sub>/CH<sub>4</sub>. *Colloids Surf. A Physico. Chem. Eng. Asp.* **2022**, *640*, 128481. [[CrossRef](#)]
143. Pu, Y.; Yang, Z.; Wee, V.; Wu, Z.; Jiang, Z.; Zhao, D. Amino-functionalized NUS-8 nanosheets as fillers in PIM-1 mixed matrix membranes for CO<sub>2</sub> separations. *J. Membr. Sci.* **2022**, *641*, 119912. [[CrossRef](#)]
144. Khdhayyer, M.R.; Esposito, E.; Fuoco, A.; Monteleone, M.; Giorno, L.; Jansen, J.C.; Attfield, M.P.; Budd, P.M. Mixed matrix membranes based on UiO-66 MOFs in the polymer of intrinsic microporosity PIM-1. *Sep. Purif. Technol.* **2017**, *173*, 304–313. [[CrossRef](#)]
145. Lee, C.S.; Kang, M.; Kim, K.C.; Kim, J.H. In-situ formation of asymmetric thin-film, mixed-matrix membranes with ZIF-8 in dual-functional imidazole-based comb copolymer for high-performance CO<sub>2</sub> capture. *J. Membr. Sci.* **2022**, *642*, 119913. [[CrossRef](#)]
146. Wu, X.; Tian, Z.; Wang, S.; Peng, D.; Yang, L.; Wu, Y.; Xin, Q.; Wi, H.; Jiang, Z. Mixed matrix membranes comprising polymers of intrinsic microporosity and covalent organic framework for gas separation. *J. Membr. Sci.* **2017**, *528*, 273–283. [[CrossRef](#)]
147. Hao, L.; Liao, K.; Chung, T. Photo-oxidative PIM-1 based mixed matrix membranes with superior gas separation performance. *J. Mater. Chem. A* **2015**, *3*, 17273–17281. [[CrossRef](#)]
148. Kinoshita, Y.; Wakimoto, K.; Gibbons, A.H.; Isfahani, A.P.; Kusuda, H.; Sivaniah, E.; Ghalei, B. Enhanced PIM-1 membrane gas separation selectivity through efficient dispersion of functionalized POSS fillers. *J. Membr. Sci.* **2017**, *539*, 178–186. [[CrossRef](#)]
149. Husna, A.; Hossain, I.; Choi, O.; Lee, S.; Kim, T. Efficient CO<sub>2</sub> Separation Using a PIM-PI-Functionalized UiO-66 MOF Incorporated Mixed Membrane in a PIM-PI-1 Polymer. *Macromol. Mater. Eng.* **2021**, *306*, 2100298. [[CrossRef](#)]
150. Sun, H.; Gao, W.; Zhang, Y.; Cao, X.; Bao, S.; Li, P.; Kang, Z.; Niu, J. Bis(phenyl)fluorene-based polymer of intrinsic microporosity/functionalized multi-walled carbon nanotubes mixed matrix membranes for enhanced CO<sub>2</sub> separation performance. *React. Funct. Polym.* **2020**, *147*, 104465. [[CrossRef](#)]
151. Sánchez-Laínez, J.; Pardillos-Ruiz, A.; Carta, M.; Malpass-Evans, R.; McKeown, N.B.; Téllez, C.; Coronas, J. Polymer engineering by blending PIM-1 and 6FDA-DAM for ZIF-8 containing mixed matrix membranes applied to CO<sub>2</sub> separations. *Sep. Purif. Technol.* **2019**, *224*, 456–462. [[CrossRef](#)]
152. Ji, Y.; Zhang, M.; Guan, K.; Zhao, J.; Liu, G.; Jin, W. High-Performance CO<sub>2</sub> Capture through Polymer-Based Ultrathin Membranes. *Adv. Funct. Mater.* **2019**, *29*, 1900735. [[CrossRef](#)]
153. Khdhayyer, M.; Bushell, A.F.; Budd, P.M.; Attfield, M.P.; Jiang, D.; Burrows, A.D.; Esposito, E.; Bernardo, P.; Monteleone, M.; Fuoco, A.; et al. Mixed matrix membranes based on MIL-101 metal-organic frameworks in polymer of intrinsic microporosity PIM-1. *Sep. Purif. Technol.* **2019**, *212*, 545–554. [[CrossRef](#)]
154. Kim, N.U.; Park, B.J.; Lee, J.H.; Kim, J.H. High-performance ultrathin mixed-matrix membranes based on an adhesive PGMA-co-POEM comb-like copolymer for CO<sub>2</sub> capture. *J. Mater. Chem. A* **2019**, *7*, 14723–14731. [[CrossRef](#)]

155. Deng, G.; Wang, Y.; Luo, J.; Zong, X.; Zhang, C.; Song, X. Synthesis and gas transport properties of hyperbranched network polyimides derived from Tris(4-aminophenyl) benzene. *Polymer* **2020**, *203*, 122776. [[CrossRef](#)]
156. Scofield, J.M.P.; Gurr, P.A.; Kim, J.; Fu, Q.; Kentish, S.E.; Qiao, G.G. Development of novel fluorinated additives for high performance CO<sub>2</sub> separation thin-film composite membranes. *J. Membr. Sci.* **2016**, *499*, 191–200. [[CrossRef](#)]
157. Hao, L.; Li, P.; Chung, T. PIM-1 as an organic filler to enhance the gas separation performance of Ultem polyetherimide. *J. Membr. Sci.* **2014**, *453*, 614–623. [[CrossRef](#)]
158. Yong, W.F.; Li, F.Y.; Xiao, Y.C.; Li, P.; Pramoda, K.P.; Tong, Y.W.; Chung, T.S. Molecular engineering of PIM-1/Matrimid blend membranes for gas separation. *J. Membr. Sci.* **2012**, *407–408*, 47–57. [[CrossRef](#)]
159. Yechan, L.; Chuah, C.Y.; Lee, J.; Bae, T. Effective functionalization of porous polymer fillers to enhance CO<sub>2</sub>/N<sub>2</sub> separation performance of mixed-matrix membranes. *J. Membr. Sci.* **2022**, *647*, 120309. [[CrossRef](#)]
160. Park, C.; Kong, C.; Kim, E.; Lee, C.; Kim, K.; Lee, J.; Moon, S. High-flux CO<sub>2</sub> separation using thin-film composite polyether block amide membranes fabricated by transient-filler treatment. *J. Chem. Eng.* **2023**, *455*, 140883. [[CrossRef](#)]
161. Jeong, I.; Hossain, I.; Husna, A.; Kim, T. Development of CO<sub>2</sub>-Philic Blended Membranes Using PIM-PI and PIM-PEG/PPG. *Macromol. Mater. Eng.* **2022**, *308*, 2200596. [[CrossRef](#)]
162. Sekizkardes, A.K.; Budhathoki, S.; Zhu, L.; Kusuma, V.; Tong, Z.; McNally, J.S.; Steckel, J.A.; Yi, S.; Hopkinson, D. Molecular design and fabrication of PIM-1/polyphosphazene blend membranes with high performance for CO<sub>2</sub>/N<sub>2</sub> separation. *J. Membr. Sci.* **2021**, *640*, 119764. [[CrossRef](#)]
163. Yong, W.F.; Li, F.Y.; Chung, T.S.; Tong, Y.W. Molecular interaction, gas transport properties and plasticization behavior of cPIM-1/Torlon blend membranes. *J. Membr. Sci.* **2014**, *462*, 119–130. [[CrossRef](#)]
164. Liu, J.; Pan, Y.; Xu, J.; Wang, Z.; Zhu, H.; Liu, G.; Zhong, J.; Jin, W. Introducing amphiphatic copolymer into intermediate layer to fabricate ultra-thin Pebax composite membrane for efficient CO<sub>2</sub> capture. *J. Membr. Sci.* **2023**, *667*, 121183. [[CrossRef](#)]
165. Han, H.; Scofield, J.M.P.; Gurr, P.A.; Webley, P.A.; Qiao, G.G. Ultrathin membrane with robust and superior CO<sub>2</sub> permeance by precision control of multilayer structures. *J. Chem. Eng.* **2023**, *462*, 142087. [[CrossRef](#)]
166. Li, S.; Wang, Z.; Yu, X.; Wang, J.; Wang, S. High-Performance Membranes with Multi-permselectivity for CO<sub>2</sub> Separation. *Adv. Mater.* **2012**, *24*, 3196–3200. [[CrossRef](#)] [[PubMed](#)]
167. Yuan, Y.; Qiao, Z.; Xu, J.; Wang, J.; Zhao, S.; Cao, X.; Wang, Z.; Guiver, M.D. Mixed matrix membranes for CO<sub>2</sub> separations by incorporating microporous polymer framework fillers with amine-rich nanochannels. *J. Membr. Sci.* **2021**, *620*, 118923. [[CrossRef](#)]
168. Gao, Y.; Quiao, Z.; Zhao, S.; Wang, Z.; Wang, J. In situ synthesis of polymer grafted ZIFs and application in mixed matrix membrane for CO<sub>2</sub> separation. *J. Mater. Chem. A* **2018**, *6*, 3151–3161. [[CrossRef](#)]
169. Li, N.; Wang, Z.; Wang, J. Biomimetic hydroxypropyl- $\beta$ -cyclodextrin (H $\beta$ -CD)/polyamide (PA) membranes for CO<sub>2</sub> separation. *J. Membr. Sci.* **2023**, *668*, 121211. [[CrossRef](#)]
170. Li, N.; Wang, Z.; Wang, J. Water-swollen carboxymethyl chitosan (CMC)/polyamide (PA) membranes with octopus-branched nanostructures for CO<sub>2</sub> capture. *J. Membr. Sci.* **2022**, *642*, 119946. [[CrossRef](#)]
171. Shen, Q.; Cong, S.; Zhu, J.; Zhang, Y.; He, R.; Yi, S.; Zhang, Y. Novel pyrazole-based MOF synergistic polymer of intrinsic microporosity membranes for high-efficient CO<sub>2</sub> capture. *J. Membr. Sci.* **2022**, *664*, 121107. [[CrossRef](#)]
172. Blunt, M.; Fayers, F.J.; Orr, F.M., Jr. Carbon dioxide in enhanced oil recovery. *Energy Convers. Manag.* **1993**, *34*, 1197–1204. [[CrossRef](#)]
173. Esposito, E.; Dellamuzia, L.; Moretti, U.; Fuoco, A.; Giorno, L.; Jansen, J.C. Simultaneous production of biomethane and food grade CO<sub>2</sub> from biogas: An industrial case study. *Energy Environ. Sci.* **2019**, *12*, 281–289. [[CrossRef](#)]
174. Carbon Dioxide (CO<sub>2</sub>) Purity Grade Chart | CO2Meter.com. Available online: <https://www.co2meter.com/en-jp/blogs/news/tagged/carbon-dioxide-co2?page=3> (accessed on 20 September 2022).
175. Iglina, T.; Iglin, P.; Pashchenko, D. Industrial CO<sub>2</sub> Capture by Algae: A Review and Recent Advances. *Sustainability* **2022**, *14*, 3801. [[CrossRef](#)]
176. Greenhouse Carbon Dioxide Supplementation. Available online: <https://extension.okstate.edu/fact-sheets/greenhouse-carbon-dioxide-supplementation.html> (accessed on 30 September 2023).

**Disclaimer/Publisher’s Note:** The statements, opinions and data contained in all publications are solely those of the individual author(s) and contributor(s) and not of MDPI and/or the editor(s). MDPI and/or the editor(s) disclaim responsibility for any injury to people or property resulting from any ideas, methods, instructions or products referred to in the content.